Catena 234 (2024) 107604

Contents lists available at ScienceDirect

Catena

journal homepage: www.elsevier.com/locate/catena

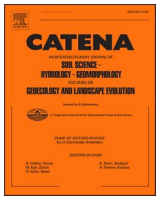

Sand subfractions by proximal and satellite sensing: Optimizing agricultural expansion in tropical sandy soils

Luis Augusto Di Loreto Di Raimo [a], Eduardo G. Couto [a], Raul R. Poppiel [b], Danilo Cesar de Mello [b], Ricardo S.S. Amorim [c], Gilmar Nunes Torres [a], Edwaldo D. Bocuti [a], Gustavo Vieira Veloso [b], Elpídio Inácio Fernandes-Filho [d], Márcio Rocha Francelino [d], José A.M. Demattê [b,*]

[a] Program in Tropical Agriculture, College of Agronomy and Zootechnology, Federal University of Mato Grosso, Cuiabá, Brazil
[b] Department of Soil, College of Agriculture "Luiz de Queiroz", University of São Paulo, Piracicaba, Brazil
[c] Department of Agricultural Engineering, Federal University of Viçosa, Brazil
[d] Department of Soil Science, Federal University of Viçosa, Brazil

ARTICLE INFO

Keywords:
Agricultural frontiers
Multispectral data
X-ray fluorescence
Sentinel
Landsat
ASTER
Sand fractions

ABSTRACT

Sandy soils, which expressly cover 7% of the Earth's land surface, are known for their management complexity and their significant influence on the proportion of sand subfractions in terms of physical, chemical, and physical-hydric properties. Proximal and remote sensing techniques offer cost-effective ways to improve soil evaluation. To address this gap, this study evaluates the potential of different sensing techniques, including laboratory-based analysis using the FieldSpec 3 spectroradiometer equipment and satellite imagery, to characterize and estimate sandy soil texture fractions and subfractions. We first defined 216 samplings in Mato Grosso State, Brazil considering the pedology, geology, synthetic soil image (exposed soil), curvature and slope of the terrain. This sampling location include sandy soils with different proportions of sand subfractions and mineralogy within a region of agricultural expansion. The sensing data used in the study were composed of total element concentrations obtained by pXRF, Vis-NIR-SWIR, and MIR spectra. The satellite data were obtained from exposed soil images of Landsat 5 and Sentinel 2, and also from simulations of Landsat 5, Sentinel 2, and Terra (ASTER). The proximal and satellite data were descriptively analysed and used to estimate the levels of clay, total sand (TS), very coarse sand (VCS), coarse sand (CS), medium sand (MS), fine sand (FS) and very fine sand (VFS). It was observed, at both the proximal and the satellite levels, that the reflectance intensity of sandy soils is inversely proportional to the particle diameter of the predominant sand subfraction. Proximal level models were slightly more accurate in predicting the texture fractions of sandy soils compared to models based on satellite data (mean validation R^2 0,45 and 0,40, respectively). In both models, SWIR and MIR stand out as key predictor variables. The results obtained in this study can be implemented to optimise the expansion of agricultural frontiers in sandy soils in other areas.

1. Introduction

Chemical and physical weathering of surface materials and soils promote change in the size and chemical constitution of their particles. In soil science, the soil fractions are usually divided for study into total sand, silt, and clay, whose proportions determine the soil texture (Bandyopadhyay et al., 2012; EMBRAPA, 2017). The texture of a soul strongly influences its chemical, physical, mineralogical,.etc. attributes, and its characterisation is critical for water management, erosion resistance, structural stability, and carbon sequestration (Krull et al., 2000; Pathak et al., 2013).

The ratio of total sand to clay is frequently used to group soils into two major classes: clayey and sandy. According to World Reference Base (FAO, 2006) soils that have > 700 g sand kg^{-1} (0.05–2.0 mm) and < 150 g clay kg^{-1} (<0.002 mm) are classified as Arenosols. Scientific studies are predominantly focused on the clay fraction of clayey soils,

* Corresponding author.
E-mail addresses: daniloc.demello@gmail.com (D.C. Mello), rsamorim@ufv.br (R.S.S. Amorim), edwaldo.bocuti@educacao.mt.gov.br (E.D. Bocuti), gustavo.v.veloso@gmail.com (G.V. Veloso), elpidio@ufv.br (E.I. Fernandes-Filho), marcio.francelino@ufv.br (M.R. Francelino), jamdemat@usp.br (J.A.M. Demattê).

https://doi.org/10.1016/j.catena.2023.107604
Received 23 April 2021; Received in revised form 26 September 2023; Accepted 17 October 2023
Available online 1 November 2023

since it is the most active constituent, while ignoring the importance of sand fractions in sandy soils (Yost and Hartemink, 2019; Di Raimo et al., 2022). However, sandy soils comprise a large territory, covering 7% of the Earth land surface (Driessen et al., 2001). In Brazil, they cover 8% of the country, and 15% across the Cerrado biome, extending mainly over agricultural areas (Donagemma et al., 2016).

Due to the constant increase in demand for food, agriculture has expanded into areas that were previously unused for agricultural, including areas with sandy soils. Brazil's latest agricultural frontier is the MATOPIBA region, which is located at the borders of the states of Maranhão, Tocantins, Piauí and Bahia, and has 20% of its area covered in sandy soils (Lumbreras et al., 2015). However, despite current research, including the Brazilian Soil Classification System (Santos et al., 2018), grouping all sandy soils together, it is known that they exhibit large variability in potential uses.

The physical, chemical, and, mainly, physical-hydric behaviours of a Sandy soil may vary, depending on the proportions of each of its sand subfractions (Donagemma et al., 2016). Zhang and Han (2019) achieved considerable increases in the water retention of sandy soils in China's Shaanxi Province by adding smaller diameter sand particles and, consequently, changing the fine-to-coarse sand ratio. Fidalski et al. (2013) observed that sandy soils with a predominance of coarse sand exhibit significantly lower water retention and availability compared to those with a predominance of fine sand in Paraná State, Brazil. Di Raimo et al. (2019), while studying sandy soils in Mayo Grosso State, Brazil, identified inversely proportional relationships between the content of coarse sand and soil erodibility values.

Traditional laboratory methods for determining the total sand, silt, and clay content of a soil, as well as the subfractions of very coarse, coarse, medium, fine, and very fine sand, require high investments of time, reagents, and financial resources (Sousa Junior et al., 2011; Viscarra Rossel et al., 2016; Demattê et al., 2019). However, recently, remote and proximal sensing techniques have been successfully used to obtain information on soils, including their characterisation, in a non-invasive, non-polluting manner, in a short period of time (Barros e Souza et al., 2021; Mello et al., 2020, 2021, 2022a,b). They have also been used to provide data in several spectral bands, providing multi-spectral information for the inference of various soil properties (Fernandes-Filho et al., 2023). Proximal soil sensing refers to the use of field-based sensors to obtain high-resolution spatial and temporal soil information by placing the sensors in contact with or close (within 2 m) to the soil (Viscarra Rossel and McBratney, 1998; Viscarra Rossel et al., 2011). Remote sensing, on the other hand, refers to the process of acquiring soil information from sensors placed more than 2 m away from the soil body.

In the last 40 years, proximally- and remotely-sensed data between 350 and 2500 nm and 4000 to 500 cm^{-1} (2500 to 25000 nm) have been used for characterising and predicting numerous soil attributes (Lacerda et al., 2016; Kopačková et al., 2017; Demattê et al., 2018a; Demattê et al., 2019; Simon et al., 2020). Like other areas of soil science research, works that focus on/study the use of remote sensing techniques in sandy soils are rare. Pereira et al. (2019) studied the capacity of proximal sensing to distinguish between various types of sandy soils but considered only total sand and used a more limited spectrum of visible and near-infrared (Vis-NIR: 350 to 1100 nm) that presents little interaction with quartz (Viscarra Rossel et al., 2006a). Fongaro et al. (2018) used proximal and remote sensors to predict clay and total sand content, but did not specify with sandy soils and their sand subfractions. Sousa Junior et al. (2011), working with a wide range of textural variation and using visible and near-infrared reflectance, near-infrared reflectance and short-wave infrared reflectance (Vis-NIR-SWIR), just subdivided the total sand fraction into coarse and fine. Viscarra Rossel et al. (2006b), Zhu et al. (2011) and O'Rourke et al. (2016) studied the ability of visible and near-infrared reflectance, near-infrared reflectance, short-wave infrared reflectance and mid-infrared reflectance (Vis-NIR-SWIR-MIR), and portable X-ray fluorescence (pXRF) to predict the attributes of soils with medium to sandy texture, but worked with total sand, silt, and clay without considering sand subfractions.

Sandy soils pose significant agricultural challenges, necessitating strict adherence to their designated suitability classes and management levels to ensure productivity. Intensive management often results in rapid degradation, demanding continuous replenishment of organic matter and nutrients, especially in tropical regions with well-distributed rainfall patterns that exacerbate soil erosion. Despite their affordability and flat terrain, sandy soils are chosen by many producers, especially when no other options are available. Prioritising fine sand over coarse sand in cultivated areas, preserving springs and watercourse banks, and avoiding residue burning are vital practices in the management of sandy soils. However, literature on their management, utilisation, and conservation is limited, due likely to the fact that they were only recently adopted in Brazil—about two decades ago (Suzuki et al., 2023). To promote sustainable usage, further comprehensive studies are needed, especially those utilizing new technologies and methods (Di Raimo et al., 2022; Silvero et al., 2023).

It is undeniable that sandy soils which occupy large extension areas globally will be the next agricultural frontier, and there is need to create a research agenda developed to use and manage these specific soils in a sustainable manner, particularly under changing climate conditions and human activities (Huang and Hartemink, 2020). Therefore, conducting research on the physico-chemical and physical-hydric behavior of sandy soils using new instruments and methods is necessary. In addition, sandy soils in Brazil have been under-studied and overlooked, as noted by Donagemma et al., (2016). There is a notable lack of research differentiating various types of sandy soils. Our study introduces methodologies utilizing non-invasive technologies to rapidly and accurately acquire information, both remotely and up close. These methodologies aim to distinguish different sandy soils by quantifying their subfractions of sand that constitute their composition. This distinction is crucial, as the prevalence of finer sand fractions primarily influences a greater specific surface area and higher cation exchange capacity. Consequently, it leads to enhanced retention of water and nutrients in the soil, which significantly impacts agricultural crop growth. This information is invaluable for effective land use planning, fertilizer management, irrigation and drainage projects, variety allocation, and overall soil management. This research will help to gain a better understanding and map the spatial variations of soil properties. Additionally, it will aid in monitoring and modeling various physical, chemical, and biological processes (Huang and Hartemink, 2020).

Given above, this research aims: *i)* to evaluate the potential and limitations of different sensing techniques (ranging from proximal to remote sensing) for the characterisation of the texture of sandy soils; *ii)* to predict the sandy subfractions of sandy soils through machine learning algorithm and evaluate the importance of variables and model performance.

Studying sandy soils using sensing technologies provides numerous advantages, such as rapid and precise quantification of various sand subfractions. These subfractions exhibit varying characteristics, including cation exchange capacity, water and nutrient retention, aeration, and susceptibility to erosion. Improved comprehension of sand subfractions benefits agriculture, sustainability, soil conservation, crop selection, water and soil fertility management, environment, economy, knowledge sharing, and climate resilience. It also aids efficient, eco-friendly farming, benefiting science and sandy-soil practitioners.

2. Methodology

2.1. Study area and sample collection

The study site covers an area of 5000 km^2 (Fig. 1), across a tropical climate region in Mato Grosso State in Midwest Brazil, that was converted to agricultural and livestock uses during the last two decades. The area has different geological formations and, is covered by Rhodic Lixisols, Rhodic Ferralsols, Haplic Cambisols, Haplic Arenosols, Gleyic

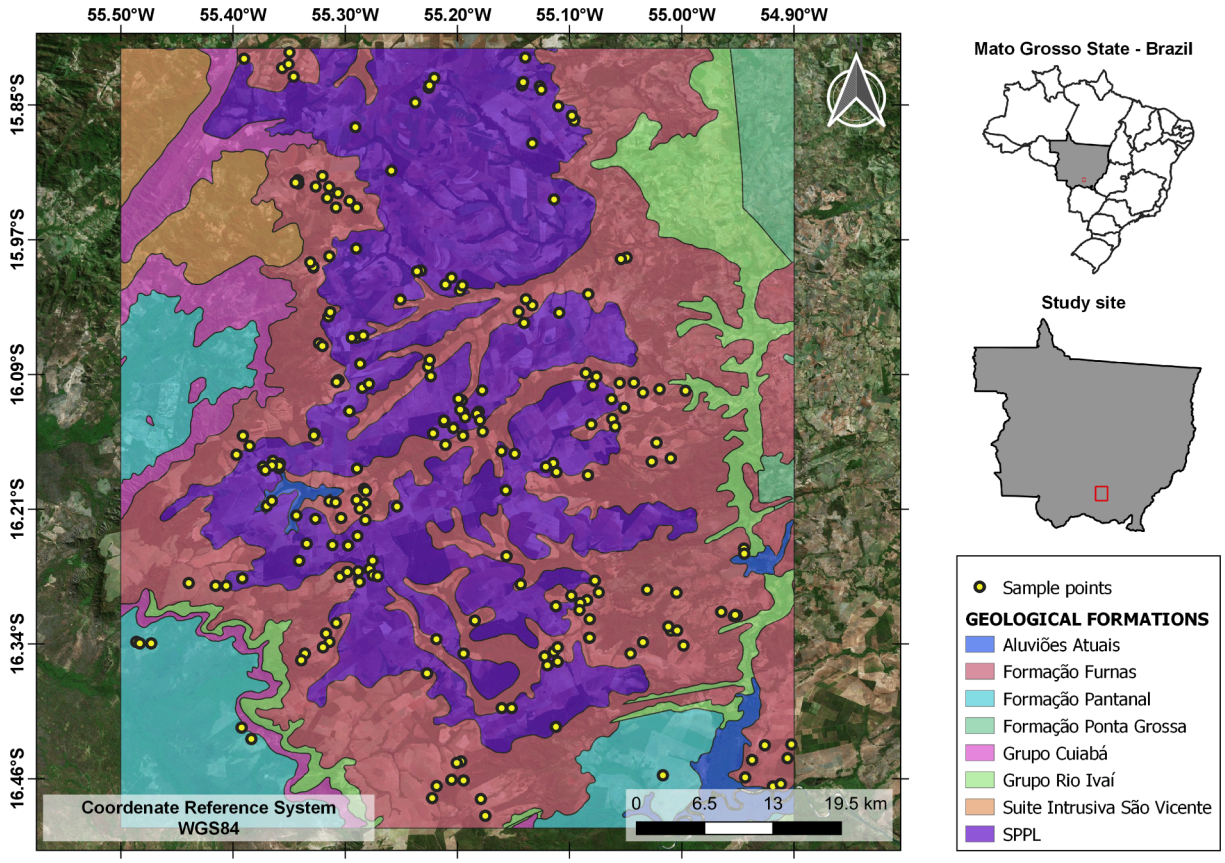

Fig. 1. Study site, sampling points and geological formations.

Arenosols and Plinthosols. The collected points are within four geological formations: Pantanal, formed by semi-consolidated and unconsolidated sandy, silty-sandy, clay-sandy and sandy-conglomerate sediments, with saline impregnations (SEPLAN, 2008); Furnas, characterised by coarse to locally fine grain quartzitic sandstone with clastic conglomerate horizons (SEPLAN, 2008); "Superfície Paleogenica Peneplanizada com Latossolizacao" (Paleogenic Peneplanized Surface with Latosolization), composed of clay-sandy soils with dark reddish-colored microaggregates and which may have a ferruginous crust at the base, rarely with solidified nodules of kaolinite on iron crust (SEPLAN, 2008); and "Aluviões atuais", formed by soil transported through water currents, and which form successive and differentiated horizons with deposits consisting mostly of sand, clays, carbonates, quartz pebbles, opals, iron sesquioxides, rusty concretions and basalt (Santos et al., 2007). In addition, the methodological flowchart is indicated in Fig. 2.

Prior to fieldwork, we performed a soil-landscape relationship analysis to understand the distribution to understand the distribution of soils into different classes and their parent materials in order to sample locations with high levels of sand and large variations between sand subfractions. The analyses of soil-landscape relationship were undertaken by soil examinations conducted along designated transects allowed for the identification of specific soil series and their correlation with landscape characteristics. An approach based on slope profiling involved categorising slopes based on variations in angular measurements taken along the transects. The inclusion of the "geomorphic surface" variable in soil-relationship interpretation is substantiated by its capacity to signify a connection between the distribution of soil across the landscape and soil age (Arruda et al., 2016).

From the soil-landscape relationship, 216 sampling locations were designated for collection at 0 to 20 cm depth intervals. The samples were dried at 45 °C for 24 h and passed through 2 mm sieves. Subsequently, following the pipette method of Teixeira et al. (2017), we determined the texture fractions: Total Sand (TS), Silt and Clay. The TS fraction was then subdivided, by sieving, into five subfractions: Very Fine Sand (VFS), Fine Sand (FS), Medium Sand (MS), Coarse Sand (CS) and Very Coarse Sand (VCS), with particle diameters ranging from 0.053 to 0.125 mm, 0.125 to 0.25 mm, 0.25 to 0.5 mm, 0.5 to 1 mm and 1 to 2 mm, respectively (Kilmer and Alexander, 1949).

2.2. Proximal sensing data

2.2.1. Visible to short-wave infrared (Vis-NIR-SWIR)

The 350–2500 nm spectral data was obtained using the FieldSpec 3 spectroradiometer, with spectral resolution of 3 nm for 350 to 700 nm and 6 nm for 700 to 2500 nm, and was automatically interpolated by the sensor for 1 nm resolution, totalling 2151 spectral bands. Samples were placed in petri dishes 8 cm from the fibre-optic sensor and 35 cm from two halogen lamps (50 W) adjusted at an angle of 30°, according to the Long Light geometry described by Romero et al. (2018). A Spectralon plate was used as a reference for calibration at fixed intervals of 20 min. The spectral curves of each sample consisted of the median value between three repeated readings, with each reading composed of an average of 15 repetitions. The petri dish was rotated at an angle of approximately 90° between each reading, in order to expose several faces of the sample to electromagnetic radiation. Splices positioned between 1000 and 1800 nm were corrected by linear interpolation of 10 bands using the "prospectr" package in the R (Stevens et al., 2020).

2.2.2. Medium infrared (MIR) and X-ray fluorescence (pXRF)

Soil samples were ground and sieved at 100 mesh for spectral measurements using the Bruker Alpha II equipment (FTIR, Bruker Inc. Billerica, MA), equipped with a diffuse reflection accessory (DRIFT). The spectra were obtained by averaging 32 consecutive readings with a spectral resolution of 2 cm^{-1}. A gold plate was used for calibration at

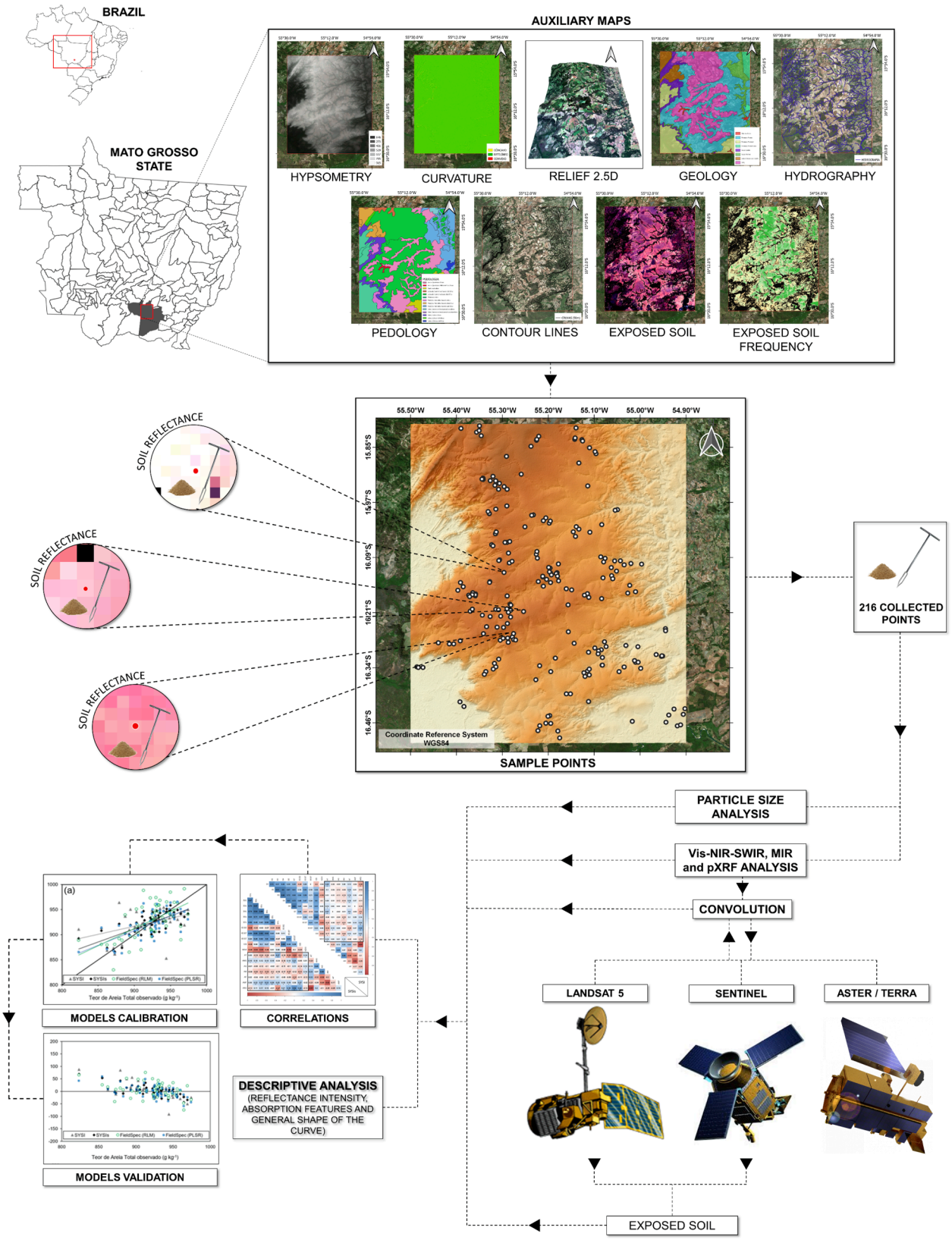

Fig. 2. Methodological flowchart of data collection and analysis procedures.

intervals of four samples analysed. Noise reflectance values between 500 and 400 cm^{-1} were removed (Jović et al., 2019). For the X-ray fluorescence analysis, the soil samples were placed in plastic bags, following the methodology presented in Silva et al. (2019). A portable fluorescence X-ray was used (pXRF), Delta Professional (Olympus ®), working in geochemistry mode.

2.3. Satellite data

Surface reflectance values were obtained using the Geospatial Soil Sensing System (GEOS3) method (Demattê et al., 2018a). These values were extracted from bare soil pixels in Landsat 5 (LS5) data spanning from 1984 to 2011, as well as Sentinel 2 (SENT) data from 2013 to 2019. For each satellite, a composite with median values of the bare topsoil reflectance was obtained by applying the Geospatial Soil Sensing System (GEOS3) method (Demattê et al., 2018a). The GEOS3 is a rule-based data-mining technique implemented within the Google Earth Engine cloud-based platform to retrieve bare soil reflectance from satellite time series for this study. This method comprises the following steps: creation of a database with Landsat 5 legacy data; filtering of the database to provide images only from the dry season in the study site; insertion of a set of rules into the system to filter other objects besides soils; calculation of Temporal Synthetic Spectral Reflectance (TESS) of the soil surface by using each bare soil occurrence for each location along the time-series; aggregation of all TESS to compose the Synthetic Soil Image (SYSI); and quantitative and qualitative validation of the SYSI through the correlation between laboratory and TESS, soil line assessment, and the principal component analysis (PCA) (Demattê et al., 2018a).

The LS5 composite contains information from 7 spectral bands of the Landsat 5 Thematic Mapper sensor, with a spatial resolution of 30 m: 450 to 520 nm (Blue), 520 to 600 nm (Green), 630 to 690 nm (Red), 760 to 900 nm (NIR), 1550 to 1750 nm (SWIR1), 2080 to 2350 nm (SWIR2) and 10,400 to 12500 nm (MIR). The SENT composite contains information from 11 spectral bands of the Sentinel 2 Multi-Spectral Instrument, with a spatial resolution of 20 m: 430 to 455 nm (Aerosol), 458 to 523 nm (Blue), 543 to 578 nm (Green), 650 to 680 (Red), 698 to 713 nm (Red Edge 1), 733 to 748 nm (Red Edge 2), 773 to 793 nm (Red Edge 3), 785 to 899 (NIR), 855 to 875 (Red Edge 4), 1565 to 1655 nm (SWIR1), and 2100 to 2280 nm (SWIR2) (Table 1).

From these composites band ratios and indices were calculated including: Red/Green, Red/SWIR1 and SWIR1/SWIR2 (Carvalho et al., 2014; Malone et al., 2009), the Normalized Difference Vegetation Index (NDVI) (Tucker, 1979) and the Grain Size Index (GSI) (Xiao et al., 2006). These indices were used as predictor variables for mathematical modelling. The values from the bare topsoil composites were extracted at each sampling location (Fig. 1).

2.4. Convolution of Landsat, Sentinel and ASTER data

The process of image convolution, or spatial filtering, involves altering the values of specific sets of pixels across the entire image to emphasize certain features by adjusting spatial frequencies. This modification is achieved using a matrix of size (m × n), which takes into account the values of neighboring pixels. Typically, the (m × m) matrix is applied across the entire image, causing changes in pixel values.

The proximal spectra between 350 and 25000 nm were convolved for spectral intervals of the Landsat 5, Sentinel 2, and Terra (ASTER), thus generating new data sets— LS5c, SENTc and ASTERc. The convolutions were performed to evaluate the potential of the spectral bands of different satellite sensors under laboratory conditions and, consequently, without the influence of atmospheric and field factors such as humidity, atmospheric aerosols, land roughness, topographic features, and others. The LS5c and the SENTc were performed using the "hsdar" R package (Lehnert et al., 2019), while the ASTERc was performed using Envi 5.3 software.

Table 1

Landsat 5 - Thematic Mapper (30 m)	
Blue	450 to 520 nm
Green	520 to 600 nm
Red	630 to 690 nm
NIR	760 to 900 nm
SWIR1	1550 to 1750 nm
SWIR2	2080 to 2350 nm
MIR	10,400 to 12500 nm
Sentinel 2 Multi-Spectral Instrument (20 m)	
Aerosol	430 to 455 nm
Blue	458 to 523 nm
Green	543 to 578 nm
Red	650 to 680 nm
Red Edge 1	698 to 713 nm
Red Edge 2	733 to 748 nm
Red Edge 3	773 to 793 nm
NIR	785 to 899 nm
Red Edge 4	855 to 875 nm
SWIR1	1565 to 1655 nm
SWIR2	2100 to 2280 nm

2.5. Data analysis

The contents of the TS, clay, silt and sand subfractions were associated using Pearson correlation, with reflectance values and indices obtained by LS5, LS5c, SENT, SENTc, ASTERc, Vis-NIR-SWIR (350 to 2500 nm), and MIR (4000 to 5000 cm^{-1}), with the contents of the total element obtained by pXRF. Mathematical models predicting soil texture parameters were calibrated and validated using 70% and 30% of the samples, respectively. In total, nine predictor models were tested: Vis-NIR-SWIR (VNS); MIR; Vis-NIR-SWIR + MIR (VNS + M); pXRF; LS5; LS5c; SENT; SENTc; and ASTERc. We selected these combinations to assess different outcomes in our predictions. Using the "AlradSpectra" software (Dotto et al., 2019), different pre-processing and modelling procedures were tested in the calibration step, aiming for the best adjustments and accuracies for the models. Subsequently, the models were applied to the validation data set. The model performances were assessed by the coefficient of determination (R^2), Root-Mean-Square Error (RMSE) and Ratio of Performance to InterQuartile distance (RPIQ).

For descriptive analysis, electromagnetic spectra from the satellite and proximal levels were grouped according to the levels of sand and its subfractions. Subsequently, mean spectral curves were generated in order to descriptively characterise and compare the similarities of shapes and reflectance intensities at different levels of data acquisition. A Principal Component Analysis (PCA) was used as a complementary analysis to observe the capacity of the Vis-NIR-SWIR and MIR to distinguish sandy soils with different textures. The spectra of pure minerals, at Vis-NIR-SWIR and MIR wavelengths, were obtained from Clark et al. (2007) for identification and comparison of patterns of sandy soils with distinct proportions of sand.

3. Results and discussion

3.1. Soil fractions and spectral patterns

Our soil dataset presented small variations for TS (56.61 to 98.46 %) and clay (5.07 to 266.60 %), and high variability in sand subfractions (92.88 to 66.08 % for FS and 53.70 to 61.87 % for VFS), as displayed in Fig. 3. Among the sand subfractions, the smallest range of variation was observed for VCS, due to its low content in highly weathered tropical soils. The soil particle size variations (Fig. 3) confirm that the environmental variables used to guide soil sampling (Fig. 1) were able to identify sandy soil with different sand subfractions.

We note that decreases in the TS content result in reductions of reflectance intensities mainly in SWIR and MIR. The change in reflectance intensity occurs at both levels of data acquisition and in all satellite sensors analysed, with emphasis on LS5 and ASTER, which present this trend in more bands (Fig. 4). Most sandy soils present higher reflectance values along the entire spectrum. The increase in sand content generates decreases in clay content, increasing the proportion of quartz/opaque minerals and, consequently, the intensity of the soil reflection (Demattê et al., 2018b; Fongaro et al., 2018; Nascimento et al., 2021). However, these differences in reflectance intensity

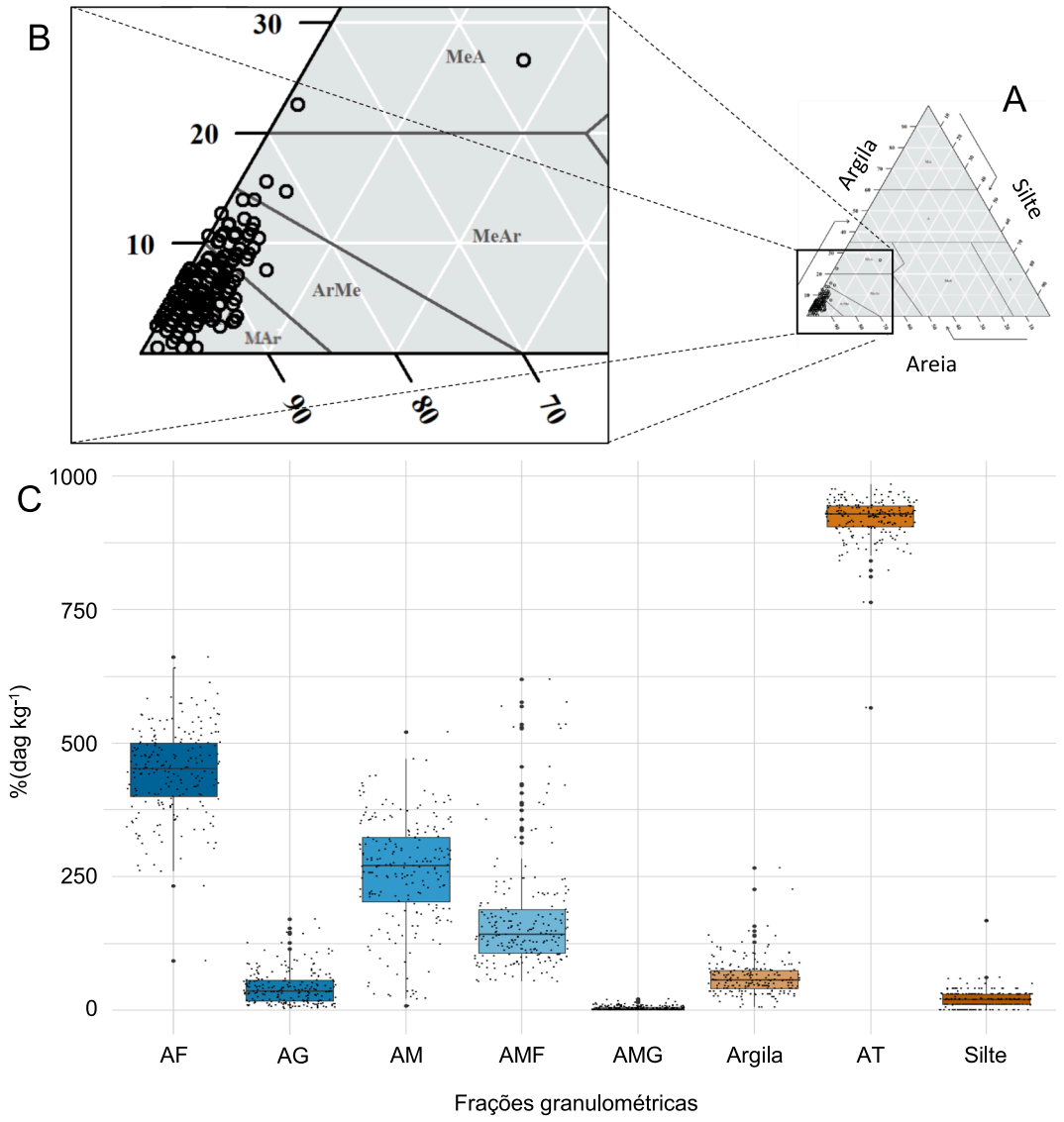

Fig. 3. A: Textural triangle; B: Sandy textural class for soil samples; C: Distribution of particle size fractions, in g kg^{-1} (TS, Total Sand; VCS, Very Coarse Sand; CS, Coarse Sand; MS, Medium Sand; FS, Fine Sand; VFS, Very Fine Sand; MeA, Clayey Medium; MeAr, Sandy Medium; ArMe, Medium Sand; e MAr, High Sandy).

between sandy soils with different TS proportions become more pronounced from the Red band on, for satellite sensors, and from 1800 nm, for laboratory spectra (Fig. 4). Fongaro et al. (2018) affirms that Landsat 5 spectra, obtained for low clay content soils, present reflectance peaks starting in red band and reaching the maximum in the SWIR1 band (1550 to 1750 nm). The same authors also affirm that as the soil clay content increases, the tendency is for the spectral shape to flatten, as is clearly observed in the LS5. Pereira et al. (2019) observed that in the SWIR the differences in reflectance intensity become clearer as the proportion of sand in the soil increases. Previous research has shown that SWIR's variability with the TS content of sandy soils is due to sensitivity to variations in particle size, metal-OH absorption bands and water molecules (Okin and Painter, 2004; Liao et al., 2013; Castaldi et al., 2016; Demattê et al., 2018b; Gasmi et al., 2019). The absorption features, located at the 1900 nm bands, are caused by the hydroxyls of water molecules within quartz minerals (Rosin et al., 2023; Viscarra Rossel et al., 2006a,b), are quite evident in sandy soils spectra, and can have great influence on the ability of SWIR to distinguish this soil type. The PCA reinforces the potential of SWIR for the distinction of sandy soils, since, alone, it has a greater ability to explain the variations in the data set than Vis-NIR-SWIR together (Fig. 5).

The differences in reflectance intensity in SWIR are also influenced by the balance between the reflectance of clay minerals and quartz. The pure quartz spectrum shows high reflectivity and flat shape in SWIR (proximal level), while the pure clay minerals (hematite, goethite and gibbsite) show high absorption in this region (Fig. 2) (Clark et al., 2007; Poppiel et al., 2020; Rosin et al., 2023). Thus, changes in sand to clay proportions of sandy soils influence the intensity of reflectance and the flat or downward trend of the curve in the SWIR region at the proximal level. Besides the intensity of reflectance, it is observed that the gibbsite features (1400 and 2200 nm) have greater depth in sandy soils with higher clay content (<800 g kg^{-1} of sand) and decrease gradually as the clay content decreases. This indicates that the clay fraction of these soils is rich in gibbsite, which was perfectly identified in this region. The orbital level spectra of the LS5, ASTER and SENT satellites were sensitive to the balance of forces between the clayey and quartz minerals, which caused changes in SWIR's reflectance intensity. However, only ASTER was able to identify changes in gibbsite features located at 2200 nm, because of its high spectral resolution in SWIR. The low spectral resolution of the ASTER sensor between 750 and 1500 nm did not allow for the identification of gibbsite features at 1400 nm. Cardoso-Fernandes et al., (2021), stated that the database containing satellite and

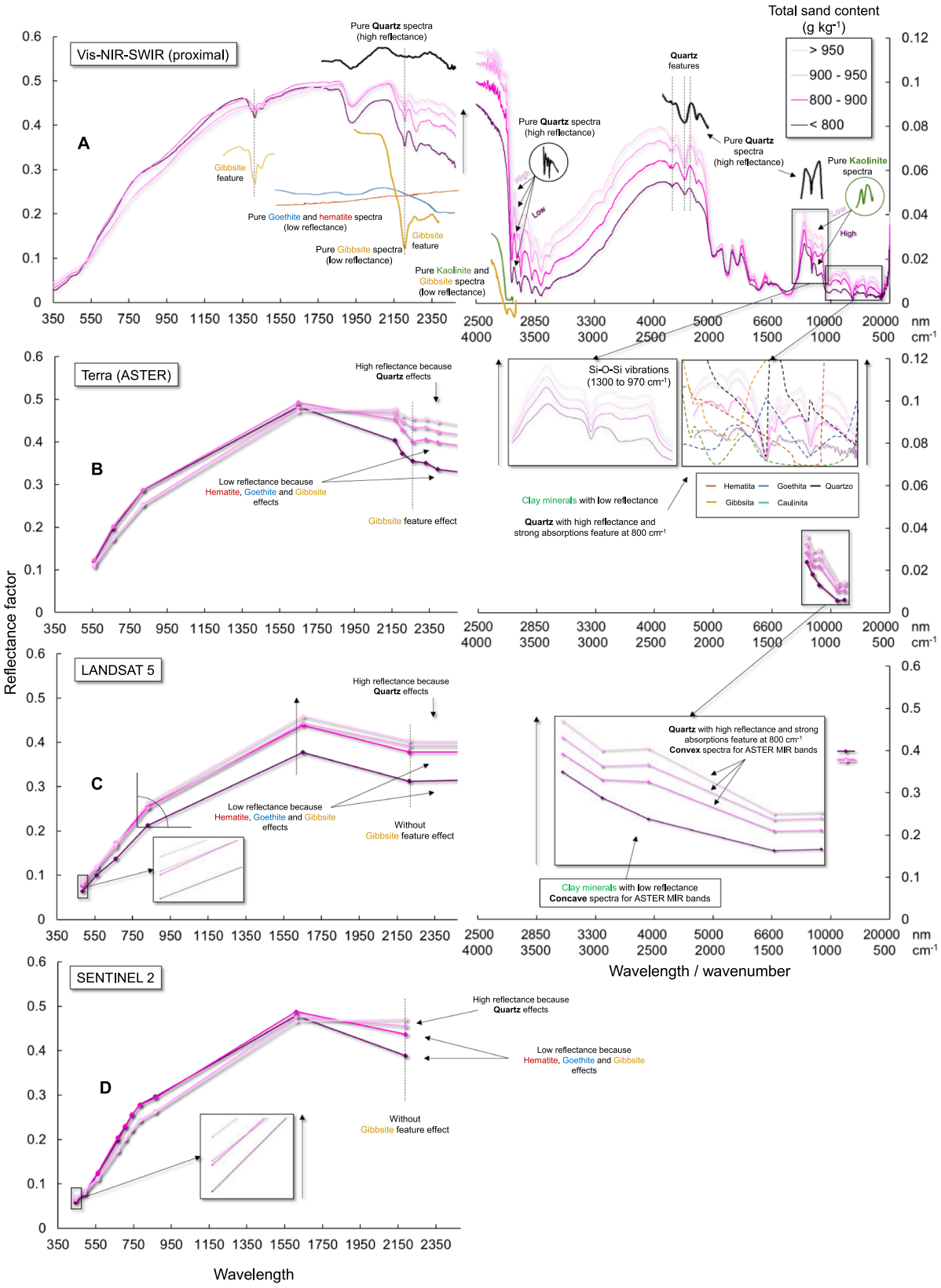

Fig. 4. Reflectance curves obtained for different Total Sand levels (in g kg^{-1}). A: at proximal level, in the Vis-NIR-SWIR and MIR regions; B: at satellite level for Terra (ASTER convolved); C: at satellite level for Landsat 5 and; D: at satellite level for Sentinel 2.

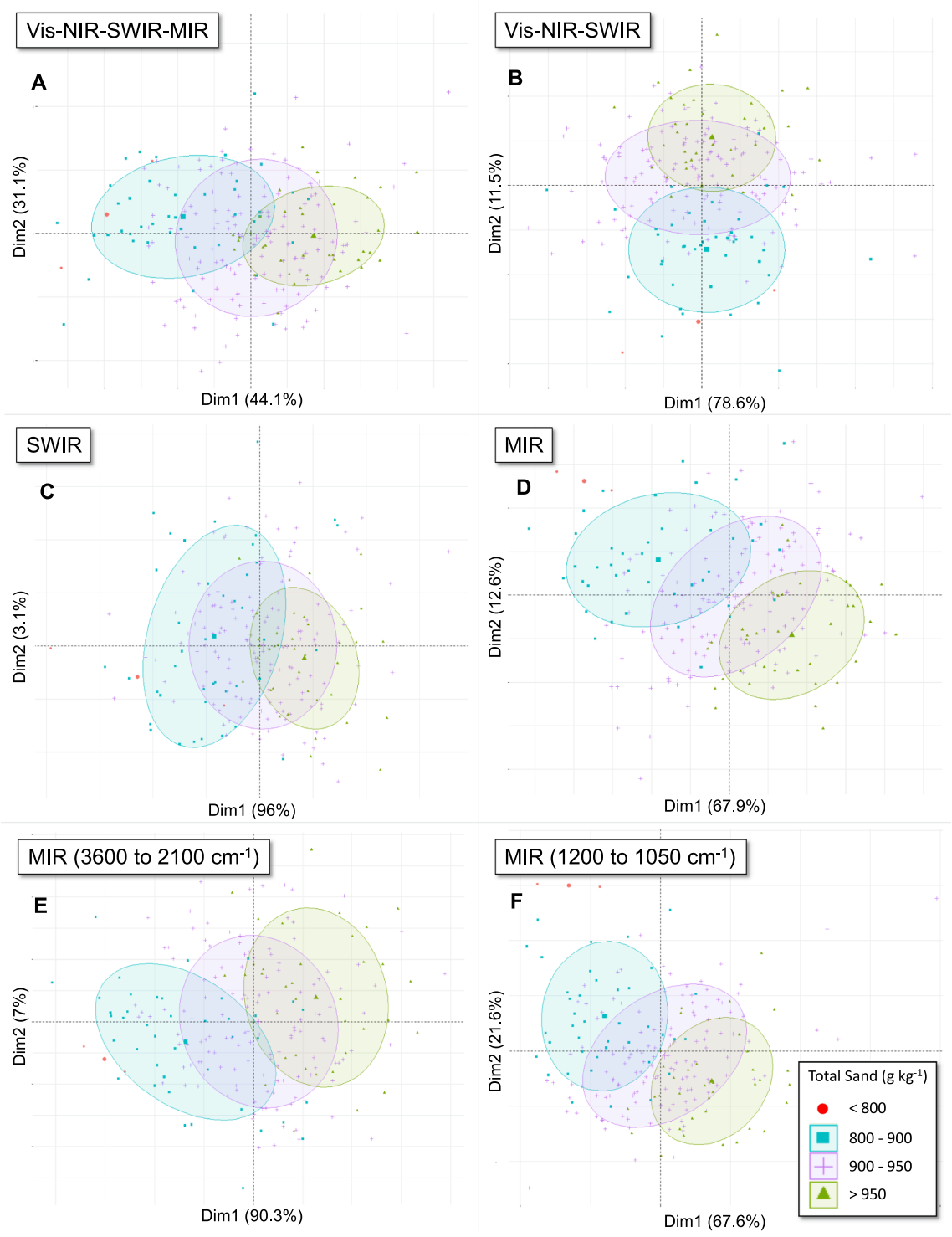

Fig. 5. Differentiation of Total Sand levels (in g kg^{-1}) through principal components analysis utilizing different regions of the electromagnetic spectrum. A: Vis-NIR-SWIR-MIR spectrum; B: Vis-NIR-SWIR; C: SWIR; D: MIR; E: MIR (3600 to 2100 cm^{-1}); F: MIR (1200 TO 1050 cm^{-1}).

laboratory spectra makes it possible to compare and evaluate the influence of the acquisition conditions on the final spectra. Furthermore, field spectra are anticipated to exhibit a closer alignment with the spectral signatures obtained through satellites.

In the MIR, the distinctions between spectral curves of different TS proportions were clearer along the entire spectrum, both at the proximal and the satellite levels, with ASTER at the latter. (Fig. 4). The single MIR band of LS5 was not able to recognise the trend of spectral variation between TS contents in sandy soils. The high capacity of MIR to distinguish soils with different proportions of TS is due to the fundamental quartz vibrations that manifest in the proximity of 1000 cm^{-1} (Demattê et al., 2022; Viscarra Rossel et al., 2006a,b), a spectral range with occurrence of Si-O-Si vibrations, and between 2500 and 1700 cm^{-1}, where quartz "overtones" are manifest (Jović et al., 2019). The PCA confirms the high capacity of MIR to distinguish soils with different TS proportions, especially the 3600 to 2100 cm^{-1} and 1200 to 1050 cm^{-1} ranges, that coincide with key absorption features (Fig. 5).

The variations in reflectance intensity between 4000 and 3250 cm^{-1}

are influenced by kaolinite, gibbsite and quartz features, and are in the ranges 2500–2000 and 1300–1050 cm^{-1} by quartz features, as observed in the spectra patterns of these pure minerals (Fig. 4) (Clark et al., 2007; Rosin et al., 2023). Sandy soils with less sand (<800 g kg^{-1}) have stronger kaolinite and gibbsite features between 4000 and 3250 cm^{-1} and, consequently, higher absorption in this region, whereas sandy soils with more sand (>950 g kg^{-1}) show marked patterns of quartz, with higher reflectivity intensities. In the ranges 2500–2000 and 1300–1050 cm^{-1} the intensity of quartz features increases proportionally from soils with less sand (<800 g kg^{-1}) to those with more sand (>950 g kg^{-1}).

Between 1000 and 500 cm^{-1}, there is a region with clear indications of the balance of forces between clay minerals and quartz (Fig. 4). Clay minerals (hematite, goethite, kaolinite and gibbsite) show higher absorption and weak features between 1000 and 500 cm^{-1}, while in this

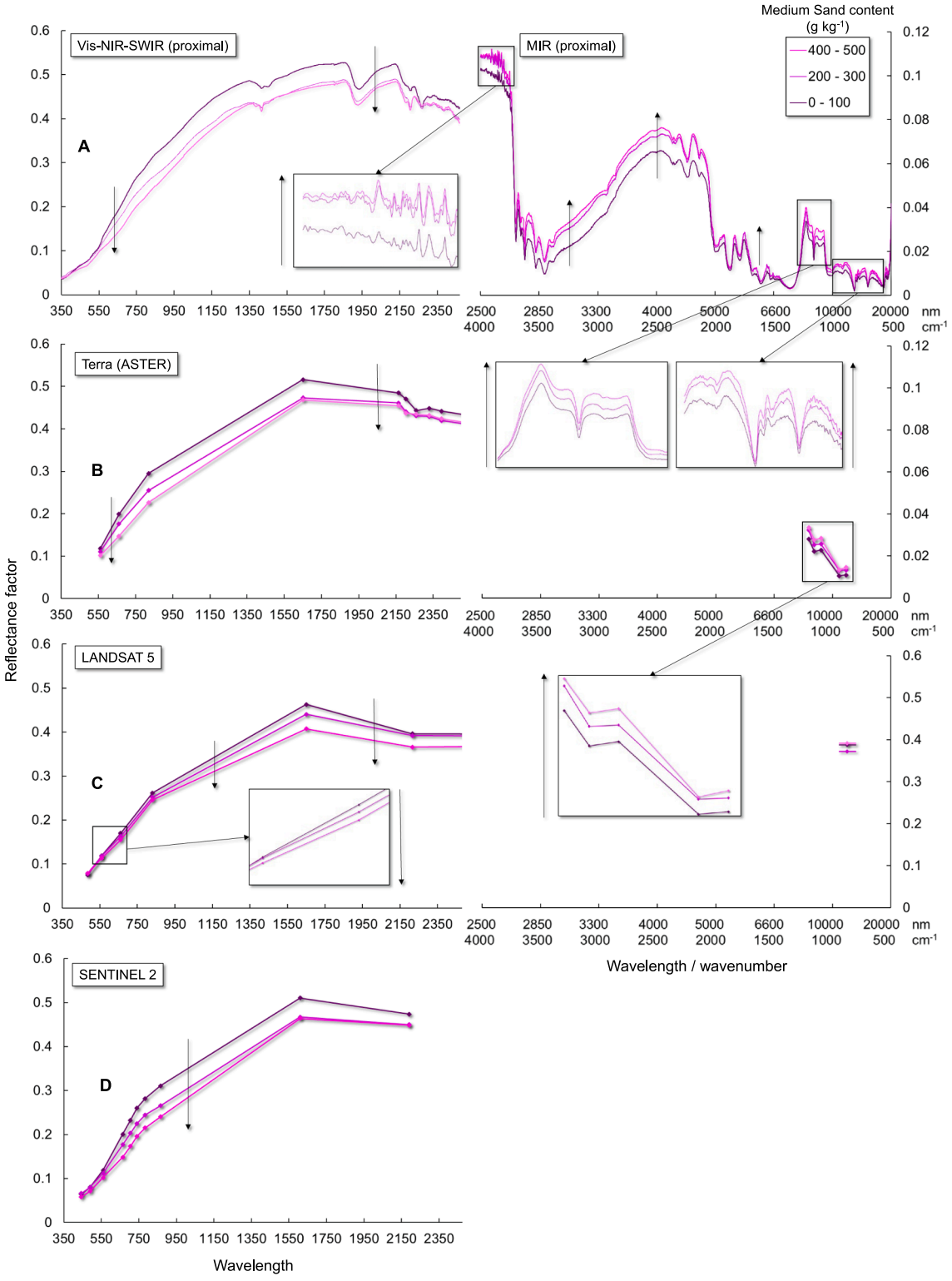

Fig. 6. Average reflectance curves obtained for different Medium Sand levels (in g kg^{-1}). A: at proximal level, in the Vis-NIR-SWIR and MIR regions; B: at satellite level for Terra (ASTER convolved); C: at satellite level for Landsat 5 and; D: at satellite level for Sentinel 2.

same region, quartz shows high values of reflectance and strong absorption feature at 810 cm^{-1}. This balance of forces between 1000 and 500 cm^{-1} coincides with the region contemplated by the MIR bands of the ASTER sensor, where it provides a slightly concave pattern in less sandy soils (<800 g kg^{-1}), which changes to convex as the sand content increases. Salazar et al. (2020) and Silvero et al. (2020) also observed the same variation of patterns in the MIR spectra of ASTER, however, working with greater contrasts between sandy and clay soils, which presented more striking patterns of concavity. These patterns identify, even in soils with small amplitudes of variation, the high potential of the ASTER sensor for characterising the texture and mineralogy of soils. Silvero et al. (2020) obtained correlation coefficients always higher than 0.72 between ASTER spectra and gibbsite, vermiculite + micas, kaolinite and iron, aluminium, silicon, and manganese oxides in the

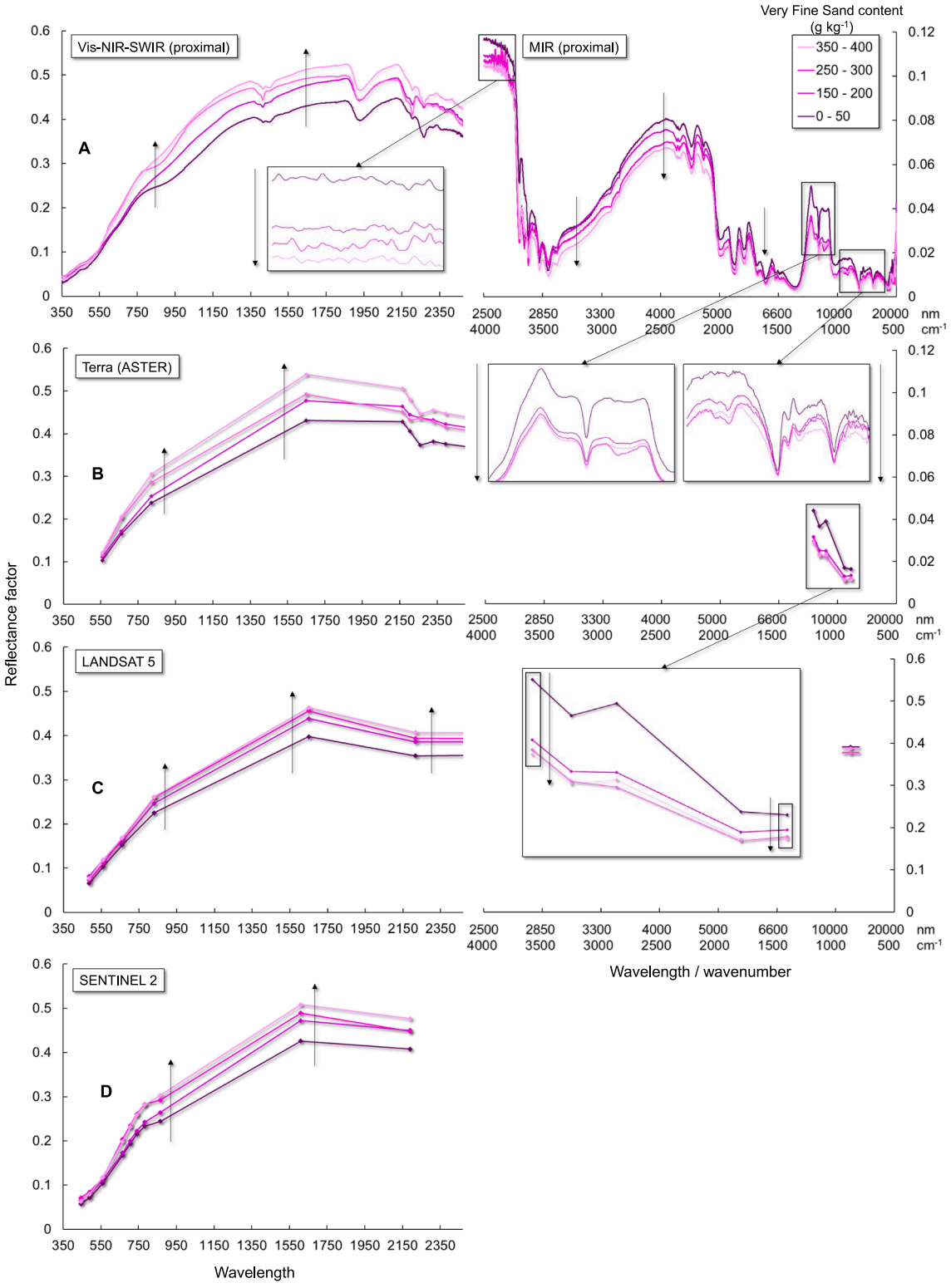

Fig. 7. Average reflectance curves obtained for different Very Fine Sand levels (in g kg^{-1}). A: at proximal level, in the Vis-NIR-SWIR and MIR regions; B: at satellite level for Terra (ASTER convolved); C: at satellite level for Landsat 5 and; D: at satellite level for Sentinel 2.

Rhodic Hapludox, Typic Hapludox, Typic Quartzipsamments, and Typic Paleudalf soils (Staff, 2017).

Figs. 6 and 7 show, respectively, the average spectral curves for increasing levels of MS and VFS subfractions, elaborated from satellite and proximal spectral data. In the Vis-NIR-SWIR it is observed that, as the proportion of MS particles increases in the soil (Fig. 6), reflectance intensities decrease. For VFS with smaller diameter particles (0,105–0,053 mm), there is an increase in reflectance intensity with the increase of their proportion in the soil (Fig. 7). This variation pattern can be visualized in both laboratory and satellite level spectra, highlighting the potential of remote sensing for the characterisation of sand subfractions in sandy soils. Okin and Painter (2004) studied the effects of changes in sand grain diameters on Vis-NIR-SWIR's reflectance in a wind erosion plume from a desert in Nizzana, Israel. The authors confirmed the findings of the present study by observing that the reflectance values were inversely proportional to the particle size predominant in different plume regions.

Larger diameter particles, when adjusted, generate larger porous spaces between them and, consequently, more dispersion paths for incident electromagnetic radiation, causing a decrease in reflectance. In contrast, smaller diameter particles adjust and provide larger contact surfaces for electromagnetic radiation, thus increasing the reflection area and reflectance values. Gomez et al., (2018) and Soltani et al. (2019) claim that fine particles, in a large proportion, increase the soil albedo, while coarse particles decrease it. According to Genot et al. (2014), the dispersion of reflected light is inversely proportional to the diameter of the particles that constitute the soil. Thus, sandy soils with predominance of larger diameter particles absorb lighter than those with fine particles in the entire spectra. According to Soltani et al. (2019), this phenomenon occurs due to the optical properties of different types of soil. In theory, soils with coarse particles cause a diffuse reflection in light, changing its direction of propagation and inducing its passage through the various materials that cause its absorption. Therefore, the decrease in the particle size of sandy soils' sand subfractions provides increased reflectance intensity (Okin and Painter, 2004; Gomez et al., 2018; Soltani et al., 2019). Consequently, it is concluded here that it is possible to distinguish between soil rich in coarse subfractions and soil rich in fine subfractions by proximal and satellite remote sensing. Ghrefat et al. (2007) concluded that it is possible to distinguish particle sizes in a dune area of White Sands using AVIRIS at the airborne level. In this study, we aim to extend their conclusion to the orbital level by utilizing LS5, Sentinel, and ASTER sensors. This finding holds great importance for the study of sandy soils, especially for the expansion of agricultural frontiers and the improvement of decision-making regarding their agricultural uses, considering that soils rich in fine particles present a completely different physical, chemical, and physical-hydric behavior from soils rich in coarse particles (Zhang and Han, 2019; Fidalski et al. 2013; Di Raimo et al. 2019).

However, it is important to note that the above mentioned pattern is only maintained when considering particles of similar mineralogy. Rosero-Vlasova et al. (2018), stated that the reduction in particle size, from sand to clay, causes a reduction in reflectance intensities, a contrary trend to that presented in the present study. However, the decrease of reflectance intensities of sand particles, generally constituted by quartz, to clay particles, constituted by opaque minerals (Fongaro et al., 2018; Rosin et al., 2023), is caused by chemical and mineralogical differences between them. This differs from the increase in reflectance intensity observed with the decrease in the sand grains diameter, attributed to the physical relationship between particles and electromagnetic radiation. Okin and Painter (2004) also evaluated the reflectance of sand particles encased in a crust of montmorillonite and hematite, and noted that the reflectance patterns vary according to the thickness of this coating, reaffirming the importance of the chemical constitution of particles in this pattern of spectral behavior.

This discussion can be furthered by analysing the inverse spectral behavior of the MIR, where, due to the grinding of soil particles in the sample preparation, the radiation-soil interaction is influenced only by chemical and mineralogical changes in the particles. In the present study, soils with lower levels of MS present had higher clay levels, while soils with lower VFS levels present had higher TS levels, a fact that justifies the inversion of reflectance trends from Vis-NIR-SWIR for MIR. These trends were observed with more clarity in the MS and VFS subfractions as a function of their greater amplitudes of variation (Fig. 3).

For the sand subfractions it was not possible to assess the mineralogical patterns of the soil, because the mineralogy and reflectance of the sand subfractions were not assessed separately. Thus, we were only able to assess and discuss general patterns of reflectance intensity conditioned by changes in the proportions of each fraction in air dried samples. Future studies will be carried out to evaluate the spectral and mineralogical behavior of each fraction separately.

3.2. Quantitative analysis

3.2.1. Correlation analysis

The correlation matrices of the predictor covariates LS5 and LS5c, SENT and SENTc, and ASTERc and pXRF are shown, respectively, in Figs. 8, 9 and 10. First, we highlight the correlation between the Red and Near Infrared Spectroscopy (NIR) bands, which represents the soil line concept and, if high, confirms that the reflectance of the data set refers to the exposed soil site (Demattê et al., 2018a; Nanni and Demattê, 2006; Poppiel et al., 2020; Silvero et al., 2021; Sullivan et al., 2005). The high and identical correlation values (0.96) observed between the Red and NIR bands of LS5 and LS5c, confirm the potential of the technique used to obtain exposed soil (Fig. 7). For SENT and SENTc, excellent results were also observed, with a correlation value of 0.94 and 0.96, respectively (Fig. 8).

The correlations between LS5 and SENT, as well as SENT and TS were both positive (0,28 and 0,26, respectively), while they were negative with the clay fraction (-0,33 and −0,43, respectively) (Figs. 8 and 9). Our results are in agreement with Liao et al., (2013), Demattê et al., (2018b) and Sayão et al. (2018). These correlation patterns occur as a function of the mineralogy commonly observed in these fractions. The TS fraction is generally composed of quartz, a mineral that presents high reflectance, while the clay fraction is composed of iron oxides and other opaque minerals, such as magnetite and ilmenite, which present high absorbance (Sullivan et al., 2005; Demattê et al., 2018b; Fongaro et al., 2018).

Analysing the convolved satellite data (LS5c, SENTc and ASTERc), it is observed that, despite good correlation values, the expected variation patterns for TS and clay were not expressed for all bands. This is because in satellite spectral data, each band reflects a mean value for that spectral band. Laboratory data spectra operate within the same spectral range as satellite data. However, when convolving this data, the results may not match the satellite mean values precisely. This discrepancy arises because the convolution process utilizes highly detailed data, rather than mean reflectance values, even though both represent the same spectral range.

This may have occurred because it was convolved information, coming from weighted means of proximal data with high spectral resolution and, consequently, with reflectance peaks and absorption bands that do not present a defined pattern when considering only the range contemplated by each sensor band.

All sand subfractions presented high correlation values with at least one of the bands or indices of satellite sensors, convolved or not. This is highlighted by the correlation values for MS and VFS, certainly due to the greater amplitudes of variation observed in these subfractions. The correlation analyses for the LS5, LS5c, SENTc and ASTER sensors also revealed inversely and directly proportional relationship patterns, with coarse and fine subfractions, respectively.

Considering the potential of the different spectral regions of satellite sensors, it is possible to highlight that the best correlation values were obtained, in general, for Vis, SWIR and MIR, as well as for the GSI, Red/

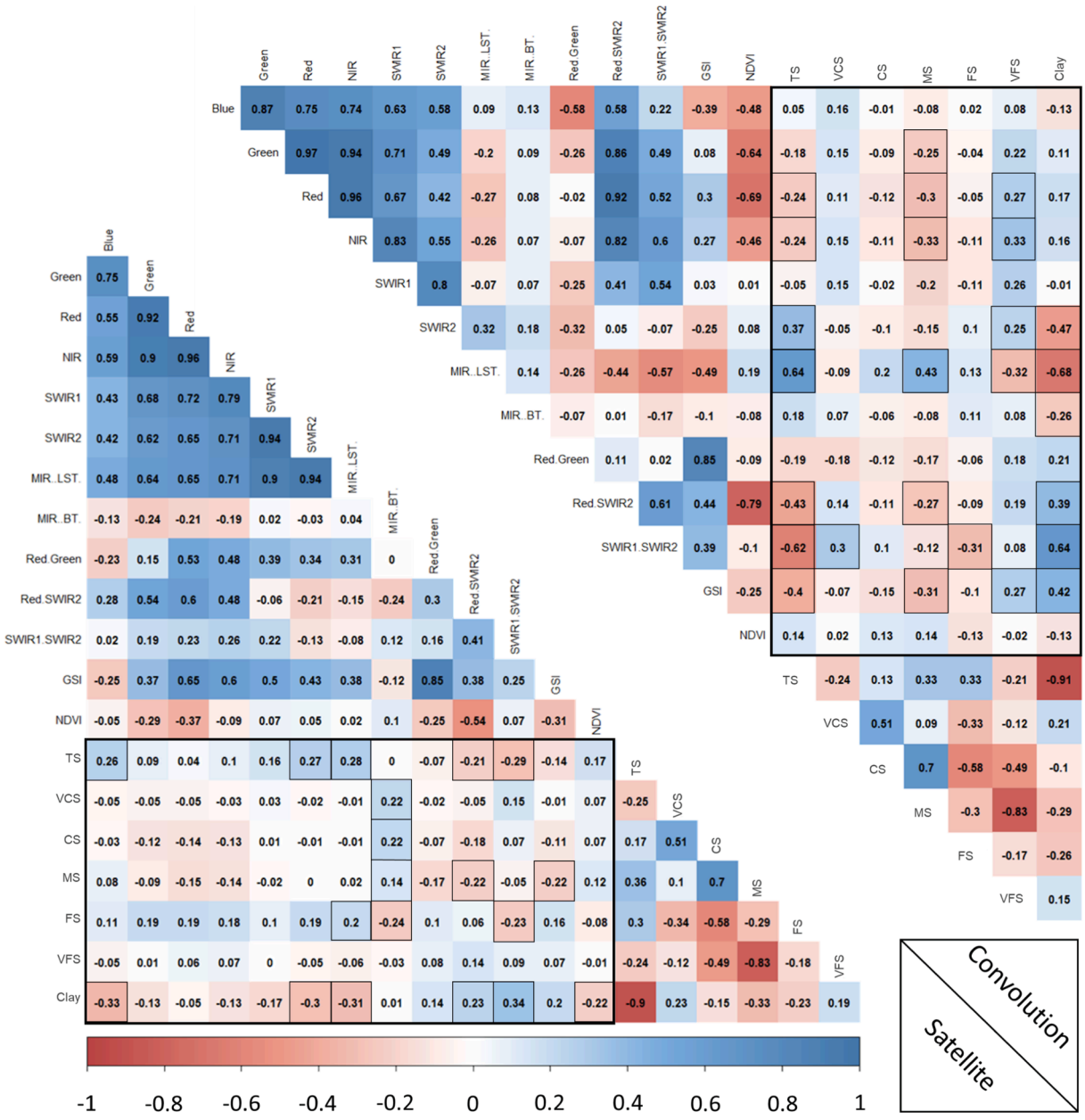

Fig. 8. Correlation matrix between LandSat, LandSat convoluted and granulometric fractions (VCS, Very Coarse Sand; CS, Coarse Sand; MS, Medium Sand; FS, Fine Sand; VFS, Very Fine Sand).

SWIR2 and SWIR1/SWIR ratios (Figs. 8, 9 and 10). Barnes and Baker (2000), Liao et al. (2013) and Fongaro et al. (2018) found that the best correlations between Landsat 5 data, satellite and convolved, and the TS and clay texture fractions occur for the SWIR1 and SWIR2 bands. Chagas et al. (2016) obtained significant correlations of Red/SWIR2, GSI and SWIR2 with the TS and clay fractions. Sousa Junior et al. (2011) and Gasmi et al. (2019), working with the ASTER sensor, observed better correlation values of the SWIR2, SWIR3, SWIR4 and SWIR5 bands with the clay, TS, CS and FS texture fractions.

Strong correlations with Vis bands may, according to Fongaro et al. (2018), be related to the influence of the high albedo of quartz, predominant in sandy soils. Correlations with SWIR bands certainly occurred due to the influence of the texture fractions in this region, since particles of different sizes, metal-OH absorption bands and water molecules cause significant changes in the reflectance values of this region (Okin and Painter, 2004; Liao et al., 2013; Castaldi et al., 2016; Demattê et al., 2018b; Gasmi et al., 2019). Regarding the MIR, the correlation results obtained here highlight and confirm the importance of this region for the analysis of sandy soils, as these regions include the main bands of quartz absorption (Hunt, 1977; Jović et al., 2019; Rosin et al., 2023; Viscarra Rossel et al., 2006a,b). Quartz is an important and prominent constituent in the composition and, consequently, in the distinction between different sandy soils types.

The results of total element contents, obtained in pXRF, showed high correlations with the particle size fractions of the sandy soils studied here (Fig. 11). The elements with the greatest ability to explain the TS and clay variations of the data set were Aluminium (Al), Silicon (Si), Titanium (Ti), Iron (Fe), Rubidium (Rb), Yttrium (Y) and Niobium (Nb), while sand subfractions were most correlated with the elements Rb, Sr, Y and Zr. The high correlations of the elements Al, Ti, and Fe with the clay fraction are due to the constituents of this textural fraction (O'Rourke et al., 2016), such as oxides of Fe, Al and Ti (hematite, goethite, Gibbsite, Titania, Titanohematite and Titanogoethite), usually found in tropical soils. Zhu et al. (2011), Wang et al. (2014), and O'Rourke et al. (2016),

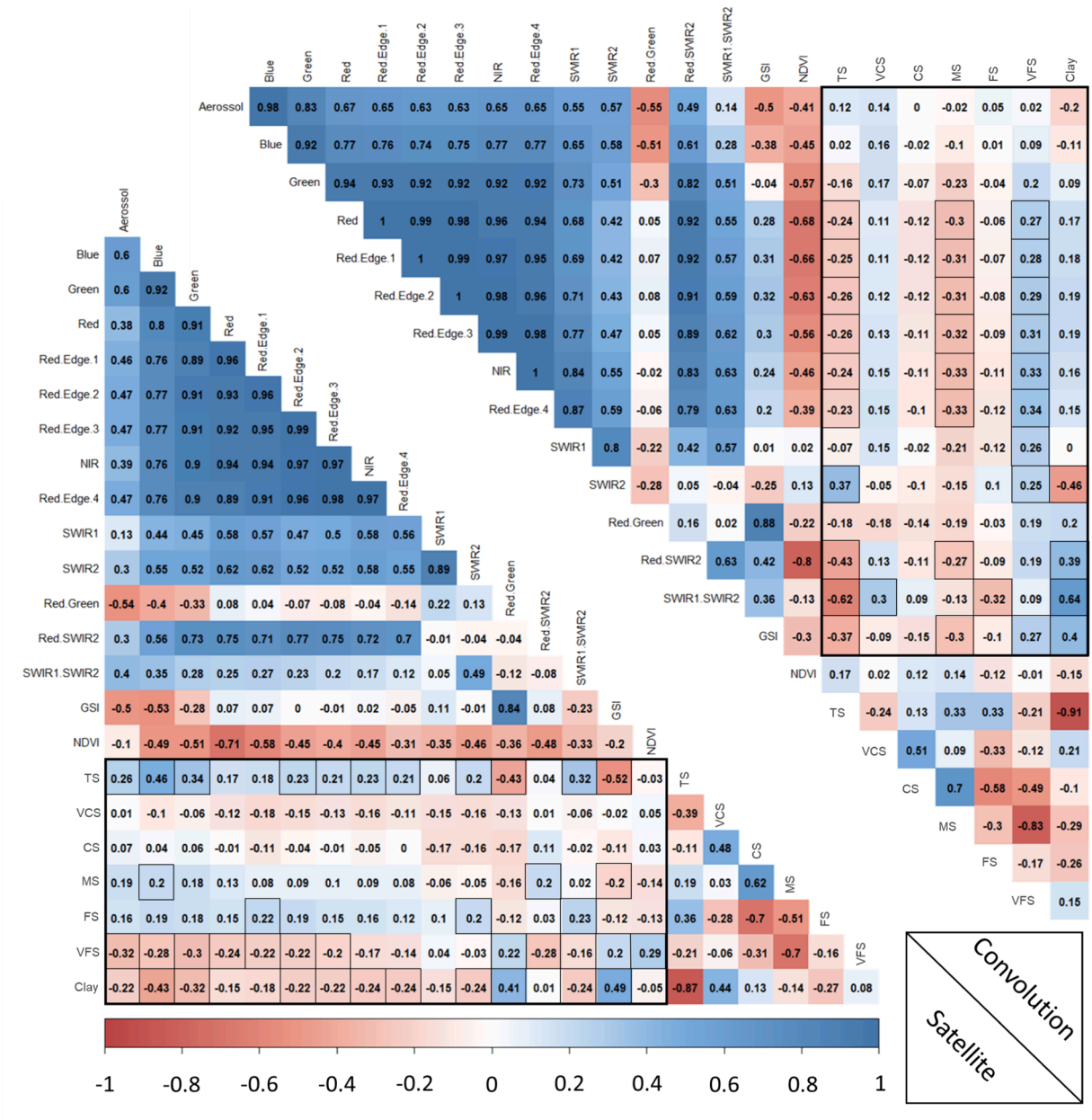

Fig. 9. Correlation matrix between Sentinel 2, Sentinel 2 convoluted and granulometric fractions (VCS, Very Coarse Sand; CS, Coarse Sand; MS, Medium Sand; FS, Fine Sand; VFS, Very Fine Sand).

in subtropical environments, also observed high correlation values of the TS and clay fractions with the Ti, Rb and Fe elements.

In the correlation analyses between texture fractions and proximal reflectance values, the variations of correlation coefficients for TS and clay present very similar patterns, with visibly higher values from 2150 nm, which comprise the SWIR and MIR (Fig. 11**).** From this region, the correlation values were mostly concentrated in the ranges −1 to −0.,6 and 0.,6 to 1. These results confirm the capacity of SWIR and MIR capacity for the characterisation of sandy soils characterization, as well as the agreement between satellite and proximal data. We observed an exact inverse pattern between the correlations of TS and clay (Fig. 11**)**, a fact also observed by Nanni and Demattê (2006). This behavior is common in tropical soils, where reductions in the contents of one of these fractions are inversely proportional to increases in the other. The high correlation value between clay and TS, obtained in the present study, confirms the inverse relationship between these fractions (Figs. 8, 9 and 10**)**.

Among the sand subfractions, the correlations remained between −0.6 and 0.6 (Fig. 11**).** Throughout the Vis-NIR-SWIR, the MS subfraction showed negative correlations with reflectance values, while the VFS subfraction showed a positive correlation. These patterns indicate, again, that the variables “sand particle size” and “reflectance intensity”“ present inversely proportional quantities, as previously discussed. As observed in the descriptive analysis of the spectra, inversions of the correlation patterns occurred from Vis-NIR-SWIR to MIR. This confirms that the effect of particle size is dominant in the Vis-NIR-SWIR, whereas in the MIR, the chemical and mineralogical characteristics dominate. This confirms that, due to the grinding of particles, the physical effect (of particles with large and small diameters) manifested in the Vis-NIR-SWIR, change for a chemical/mineralogical effect in the MIR. This change attenuates the highest levels of clay (opaque minerals) and sand (quartz) in the soils, instead of the particle size. When we analyse the TS and clay fractions, this inversion of patterns does not occur. This observation confirms the theory of chemical/mineralogical effect in

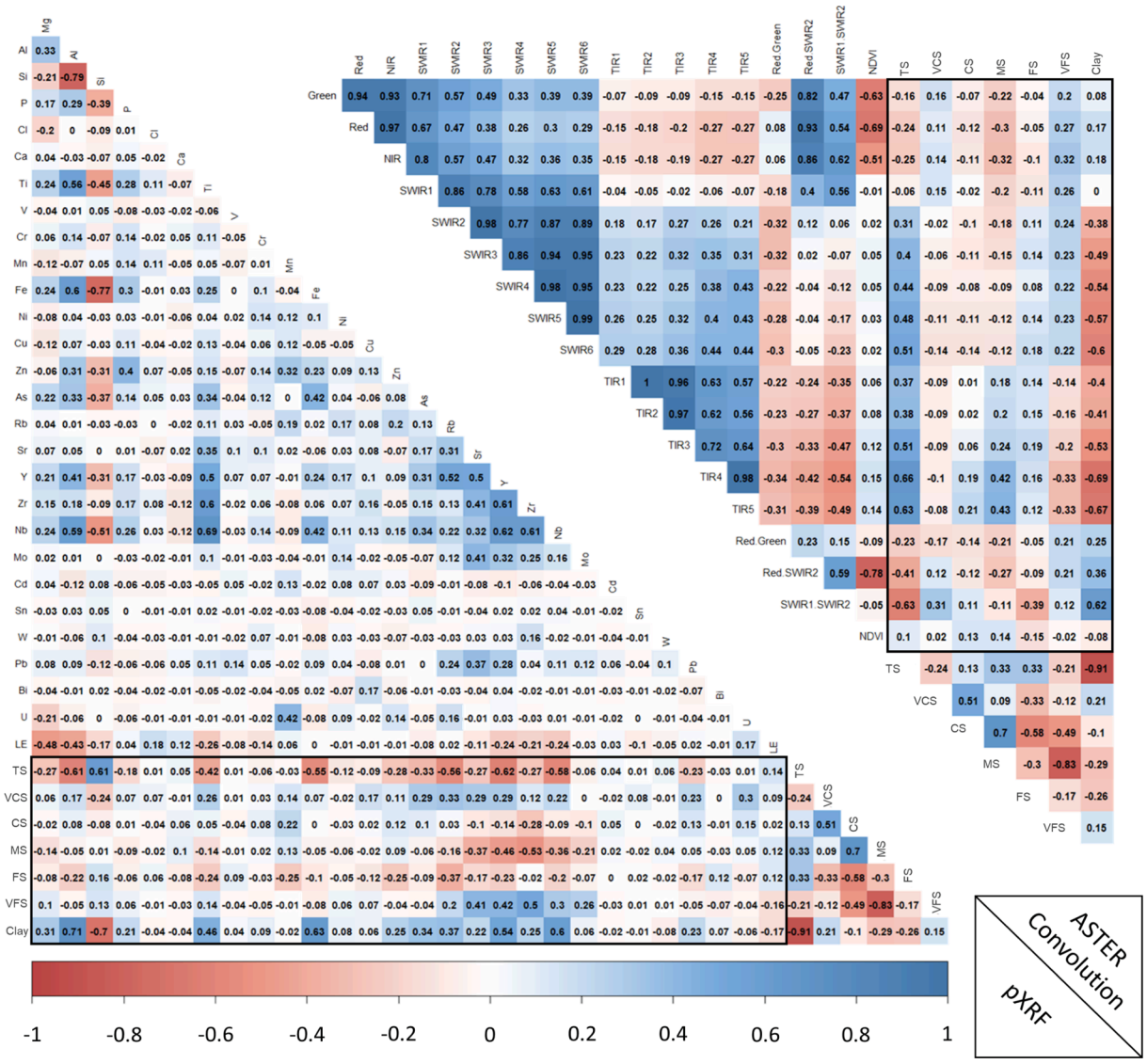

Fig. 10. Correlation matrix between ASTER convoluted, pXRF and granulometric fractions (VCS, Very Coarse Sand; CS, Coarse Sand; MS, Medium Sand; FS, Fine Sand; VFS, Very Fine Sand).

MIR, since the relationship between TS and clay is always negative.

3.2.2. *Predictive analyses*

After testing different pre-processing and modeling techniques for model elaborations, we observed, for the satellite level data that the best adjustments were made using a Support Vector Machine (SVM) model with a radial kernel. Probably because SVM is less impacted by soil sample size and class imbalance than other ML algorithms (Thanh Noi and Kappas, 2017). Gholizadeh et al. (2018) also tested model types for satellite data and found better predictive performance of texture fractions using SVM. The authors attributed this fact to the high capacity of the method to generate nonlinear adjustments, consistent with the relationship between soil attributes and satellite level reflectance values. In addition, Cardoso-Fernandes et al., (2020) stated that SVM may indicate more overtraining and lesser ability to generalise to unknown data during the modeling process, which can contribute to model performance. For the Vis-NIR-SWIR and MIR data, the best modelling method was Partial Least Square Regression (PLSR), currently considered the standard for spectrum modelling (Rosero-Vlasova et al., 2018) because of its ability to reduce collinearity between reflectance values. The pXRF data was best fit using a Random Forest model. The different pre-processing methods tested did not provide increased accuracy in the mathematical models.

Fig. 12 displays R^2, RMSE, and RPIQ values for the calibration and validation datasets. All the texture fractions studied showed correlations with at least one of the predictor variables of both the proximal and the satellite levels. Fig. 13 shows the scatter plots of observed and predicted values for the calibration and validation datasets, as well as the importance of the variables in the models. This information was presented only for the best models at each level (proximal and satellite) obtained for each textural fraction.

For the TS fraction the best performance at the proximal level was obtained by VNS + M, and at the satellite level by ASTERc (Fig. 12**).** At the proximal level, the SWIR bands were more important to the adjustment of the model than the entire MIR (Fig. 13**).** Possibly, this result can be attributed to the high content of TS in soils, which caused high homogeneity in the mineralogical constitution of the samples and, consequently, increased the importance of the SWIR, that is sensitive to particle sizes (Okin and Painter, 2004). At the satellite level, in spite of the importance of the SWIR, specifically bands SWIR5 and SWIR6, and the SWIR1/SWIR2 index, the MIR showed the greatest weight overall within the model (Fig. 12).

As for the clay fraction, the VNS + M and ASTERc models performed best at the proximal and satellite levels, respectively (Fig. 12**).** Similar to

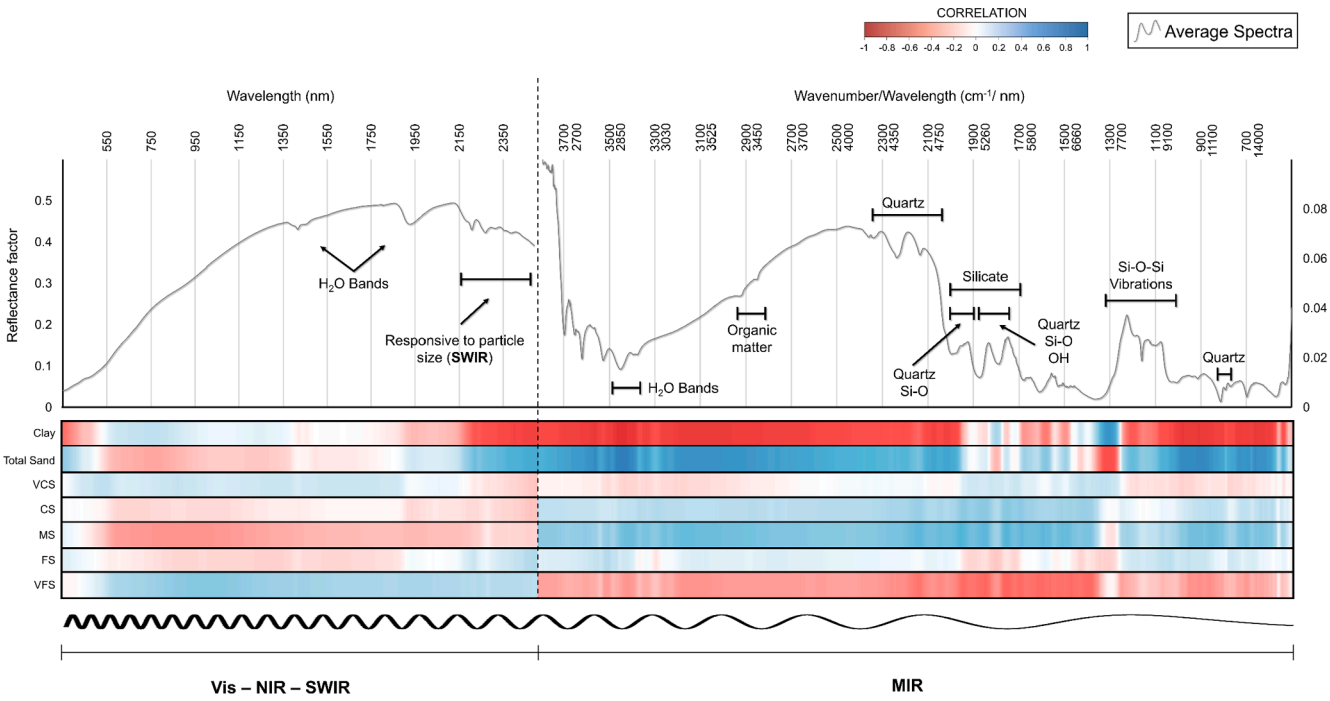

Fig. 11. Correlation between reflectance values in Vis-NIR-SWIR and MIR regions and granulometric fractions (VCS, Very Coarse Sand; CS, Coarse Sand; MS, Medium Sand; FS, Fine Sand; VFS, Very Fine Sand).

TS, SWIR was more important than MIR for clay models, and showed even more prominence compared to that observed for the TS fraction. However, the peaks close to 8000 and 20000 nm were of increased importance for clay prediction (Fig. 13), possibly due to the sensitivity of this region in identifying quartz. Quartz normally presents an inversely proportional relationship to the level of clay in the soil (Poppiel et al., 2020; Viscarra Rossel et al., 2006a,b). The relative importance of the ASTERc variables for predicting clay fraction were very similar to those observed for TS.

For VCS the best accuracy was observed for pXRF, at the proximal level, and for LS5c, at the satellite level (Fig. 12). The elements Fe, U, Ti, Rb, Sr and Y were most important within the pXRF model, with amounts always higher than 70% (Fig. 13). For the LS5c sensor, the MIR and SWIR regions were of greatest importance, particularly the SIWR1/SWIR2 index. The CS subfraction predictions were best done using VNS + M and LS5c at the proximal and satellite levels, respectively. The most important regions within the VNS + M were SWIR and MIR (±20000 nm) and, for the LS5c sensor, the MIR band (Figs. 12 and 13).

The VNS + M, for proximal level, and ASTERc, for satellite level, were the best variables for MS prediction (Fig. 11). Again, SWIR and MIR (±20000 nm) were most important within the proximal model, while the MIR4 and MIR5 bands were most important for the satellite sensor (Fig. 11). At the proximal level, none of the predictor variables presented good statistical parameters for FS prediction, however, good results were obtained for the satellite level sensor LS5, specifically the indices SWIR1/SWIR2 (74%) and Red/SWIR2 (100%) (Figs. 12 and 13).

At the proximal level, the VFS subfraction was better predicted using VNS + M and, again, the patterns of variable's importance pointed to the high contribution of SWIR and MIR (±20000 nm) (Figs. 12 and 13). Among the satellite sensors, LS5c estimated with greater accuracy the VFS subfraction. In addition to the MIR band, observed as an important variable for the prediction of other sand subfractions, the Green, Red and NIR bands, as well as the GSI index, showed greater influence on the model adjustment.

For proximal-level sensors evaluated, the excellent results obtained for VNS + M are unquestionable, as it is the best model for six of the seven texture fractions analyzed. Viscarra Rossel et al. (2006b) also found better predictive capabilities for sand, silt and clay using VNS + M, compared to Vis, NIR-SWIR and MIR separately. The performance of individual proximal sensors VNS, MIR and pXRF were overshadowed by the excellent results of VNS + M, however, they are also good predictors of sandy soil texture fractions (Fig. 12). Among the satellite sensors, ASTERc and LS5 were highlighted. The SENT satellite sensor, despite good predictive capabilities for most of the texture fractions (Fig. 12), never led to the best model. Possibly, this was due to the absence of a MIR band, a region that, in the present study, proved to be very important for estimating texture fractions of the sandy soils.

Predictor variables of high importance are predominantly contained in the SWIR and MIR. This pattern again confirms the importance of these regions for characterization and modelling of sandy soil attributes, precisely because of their sensitivity to identify particles of different sizes, metal-OH absorption bands, water molecules, quartz, Si-O-Si, silicates and H_2O of crystalline structures (Okin and Painter, 2004; Liao et al., 2013; Castaldi et al., 2016; Demattê et al., 2018b; Gasmi et al., 2019; Hunt, 1977; Viscarra Rossel et al., 2006a; Jović et al., 2019). The importance of visible bands (Red, Green and the related GSI Index) for predicting texture fractions of sandy soils, specifically the finer ones, may be related to the influence of quartz and fine particles in the soil albedo (Fongaro et al., 2018; Gomez et al., 2018).

Throughout the present study it was possible to observe that the models obtained with the sensor at the proximal level were, in general, more accurate than those at the satellite level. Such superiority could be attributed only to the controlled conditions offered by the laboratory (Demattê et al., 2007a,b; Gallo et al., 2018; Demattê et al., 2018b; Fongaro et al., 2018). However, from the important analysis of the predictor variables, it is concluded that the spectral resolution in the SWIR and MIR, little explored by Landsat and Sentinel, are of extreme importance for the prediction of texture fractions in sandy soils.

Sousa Junior et al. (2011) and Gasmi et al. (2019), used the ASTER sensor, which presents six bands in the SWIR and five in the MIR, for texture fractions prediction and also obtained excellent results. Gomez et al. (2018) obtained better predictive performance of texture fractions using the ASTER sensor in relation to Landsat and Sentinel 2. Multiple authors have therefore concluded that the development of satellite

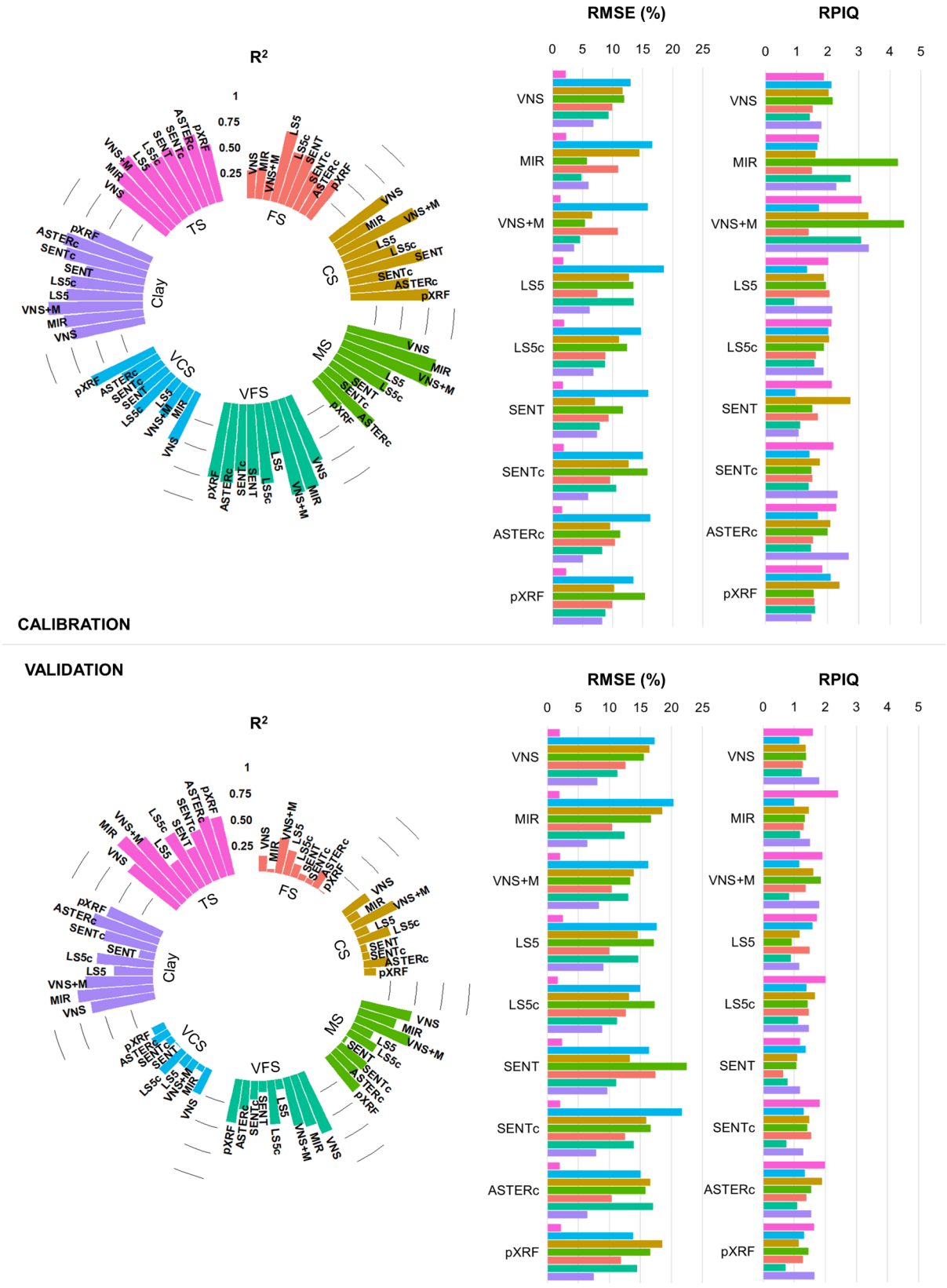

Fig. 12. Performance of models using satellite and proximal level remote sensing parameters to predict granulometric fractions.

sensors with increasing spectral resolution and increasing band specificity are key to the improvement in large-scale soil attribute characterisation, and thus contribute to sustainable land use (Demattê et al., 2007a,b; Fongaro et al., 2018)). With this in mind, Silvero et al. (2020) concluded that in the near future, new sensors applying to soil science would benefit from new spectral regions, highly rich in mineralogical constituents and soil attributes.

Works using satellite sensors to estimate TS and clay fractions were

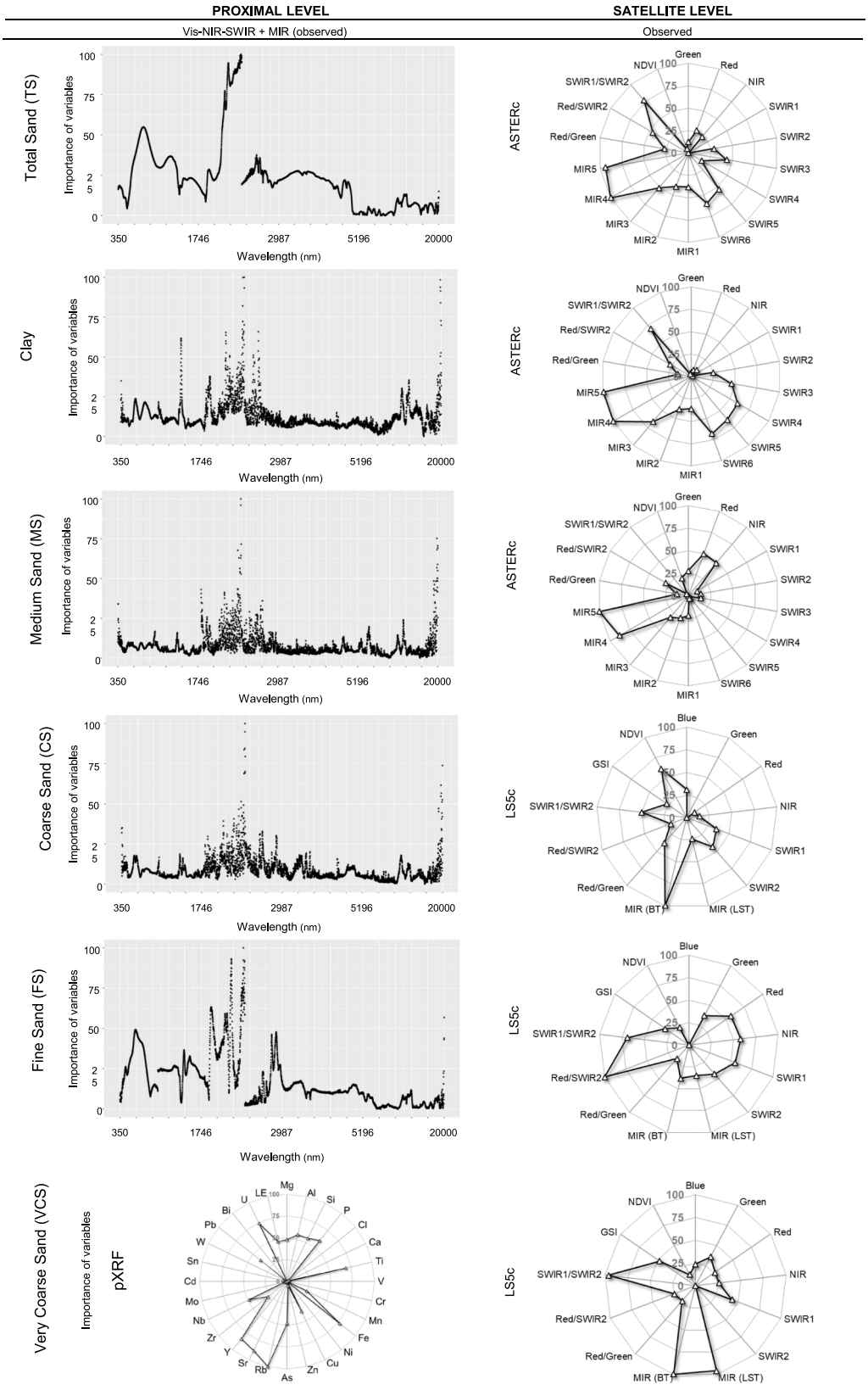

Fig. 13. The best proximal and satellite level models for entire sand subfractions and clay prediction.

developed by Liao et al. (2013), Chagas et al. (2016) and Sayão et al. (2018) with Landsat 5, Demattê et al. (2007a,b) with Landsat 7, Rosero-Vlasova et al. (2018) and Gomez et al. (2018) with Sentinel 2, ASTER, Landsat 8 and Landsat 7 simulations. These authors obtained models with R^2 values approximately 0.8 for most of the soil attributes analysed, which are generally lower than those obtained in the present study. Even with sensors located miles away from the soil surface, having a spatial resolution between 20 and 30 m, low spectral resolution, and being

exposed to moisture and atmospheric conditions (Demattê et al., 2007a, b; Gallo et al., 2018; Demattê et al., 2018b), the satellite level models presented performance very close to those generated with convolved laboratory data (Fig. 12). This is despite the fact that laboratory data was obtained in a controlled environment and with high spectral resolution (Fongaro et al., 2018). The present results highlight the capacity of satellite data, not only for the characterisation, but also for the modelling of the texture fractions of sandy soils in large areas.

Nanni and Demattê (2006) concluded that convoluted laboratory data was always better than satellite data for predictive models due to certain soil factors, such as moisture and the occurrence of crusts. However, the limitations found by Nanni and Demattê (2006) may be related to the origin of their satellite data, extracted from a single image, and the process used to identify exposed soil pixels. In the present work, satellite information was obtained from a historical series of 27 years, for Landsat, and 7 years, for Sentinel 2, with efficient and diversified ways of identifying exposed soil pixels. These results highlight the evolution of remote sensing techniques and their growing benefits to soil science.

Among the sand subfractions, it can be observed that the models with the best accuracy were obtained for MS and VFS, precisely those with the greatest variation. Demattê et al. (2007a,b), Gomez et al. (2012), and Chagas et al. (2016) affirms that data sets with large variation provide more accurate models. Sousa Junior et al. (2011) generated models for CS and FS subfractions, using reflectance values from the ASTER sensor, and obtained good accuracy for the CS subfraction, which ranged from 0 to 700 g kg^{-1}.

The results of the present study will hopefully lead to more complex models that will allow for mapping the spatial variability of sandy soils over large areas, similar to the work of Liao et al. (2013), Fongaro et al. (2018) and Sayão et al. (2018). The analysis of spectral behavior specific to combinations of particle size and mineralogical composition related to different sandy soil profiles will also be critical to further the understanding of the complexity and variability of sandy soils.

3.2.3. Study limitations and recommendations

The main limitations of this study were related to: limited applicability in vegetated areas, changing policies, dependency on field data, incomplete elimination of strawman, limited impact of strawman effect, lack of discussion on model generalisability, absence of statistical data, and spectral similarity of straw and soil.

At an orbital level, images featuring exposed soil exhibit high accuracy when utilized in regions with agricultural activities that have disrupted and uncovered the soil. Conversely, areas with native vegetation lack a significant history of soil exposure, making it challenging to generate images of exposed soil. It is worth noting that both national and international public policies are increasingly focused on preserving vegetation cover in agricultural regions. As a result, this technique is likely to become more limiting in the near future. The modelling of a particular attribute relies heavily on field data, which implies that a single universal model is highly improbable. Instead, specific regional models would be more feasible.

An integral aspect of the methodology involves mitigating the strawman effect. While GEOS3 substantially reduces this effect, it does not completely eliminate it. This is because the spectral signature of straw often resembles that of sandy soils. Consequently, if the filter allows straw to pass through, it may indicate the presence of either sandy or clayey soil at the site. Nevertheless, this observation has been found to have a limited impact.

4. Conclusions

Based on our findings, we observed an inverse relationship between the Vis-NIR-SWIR reflectance intensity of sandy soils and the grain diameter of the predominant sand subfraction, a pattern evident at both proximal and satellite levels. In contrast, the MIR spectrum reflects the chemical/mineralogical effects more prominently, resulting in reversed reflectance patterns. The SWIR and MIR bands prove pivotal in characterising and predicting sandy soil texture fractions. The ASTER satellite exhibits significant potential in distinguishing texture classes and mineralogical compositions of sandy soils. Proximal models exhibit slightly higher accuracy in predicting the texture fractions of sandy soil compared to satellite models, with similar accuracy between standard and convolved satellite models. This demonstrates the strong capabilities of satellite sensors for predicting the total sand (TS) content, clay content, and sand subfractions of sandy soils. Notably, the most accurate predictions for sand subfractions, regardless of data acquisition level, were achieved with MS and VFS data. These findings signify a major advancement in soil science, enabling the optimisation of agricultural expansion into sandy soils with varying particle compositions, which exhibit distinct physical, chemical, and hydrological behaviors.

5. Declaration of generative AI and AI-assisted technologies in the writing process

Statement: During the preparation of this work, the authors utilized GPT-4 to correct the grammar and structure of the English language, ensuring clarity in the sentences for the reader. After using this tool/service, the author reviewed and edited the content as needed and take full responsibility for the content of the publication.

Declaration of Competing Interest

The authors declare that they have no known competing financial interests or personal relationships that could have appeared to influence the work reported in this paper.

Data availability

The authors do not have permission to share data.

Acknowledgements

This study was financed in part by the “Coordenação de Aperfeiçoamento de Pessoal de Nível Superior – Brasil” (CAPES) – Finance Code 001. We would like to thank the São Paulo Research Foundation (FAPESP) (grant No. 2014-22262-0) for providing essential resources to the Laboratory of Remote Sensing Applied to Soils from “Luiz de Queiroz” College of Agriculture (ESALQ/USP); and the Geotechnologies in Soil Science group (GeoSS – website http://esalqgeocis.wixsite.com/english) for the support.

References

Arruda, G.P.d., Demattê, J.A.M., Chagas, C.d.S., Fiorio, P.R., Souza, A.B.e., Fongaro, C.T., 2016. Digital soil mapping using reference area and artificial neural networks. Sci. Agric. 73 (3), 266–273.

Bandyopadhyay, K., Aggarwal, P., Chakraborty, D., Pradhan, S., Garg, R.N., Singh, R., 2012. Practical Manual on Measurement of Soil Physical Properties. Div. Agric. Physics, Indian Agric. Res. Institute, New Delhi-110012, India 62.

Barnes, E.M., Baker, M.G., 2000. Multispectral data for mapping soil texture: possibilities and limitations. Appl. Eng. Agric. 16, 731–741. https://doi.org/10.13031/2013.5370.

Barros e Souza, A., Demattê, J.A.M., Bellinaso, H., Mello, D.C.d., da Silva Lisboa, C.J., de Oliveira Mello, F.A., Marques, K.P.P., de Resende, M.E.B., Reis, J.V., Mancini, M., Silva, S.H.G., Curi, N., 2021. A sensors-based profile heterogeneity index for soil characterization. Catena 207, 105670.

Cardoso-Fernandes, J., Teodoro, A.C., Lima, A., Roda-Robles, E., 2020. Semi-Automatization of Support Vector Machines to Map Lithium (Li) Bearing Pegmatites. Remote Sens 12 (14), 2319. https://doi.org/10.3390/rs12142319.

Cardoso-Fernandes, J., Silva, J., Dias, F., Lima, A., Teodoro, A.C., Barrès, O., Cauzid, J., Perrotta, M., Roda-Robles, E., Ribeiro, M.A., 2021. Tools for Remote Exploration: A Lithium (Li) Dedicated Spectral Library of the Fregeneda-Almendra Aplite–Pegmatite Field. Data 6 (3), 33. https://doi.org/10.3390/data6030033.

Carvalho, W., Lagacherie, P., da Silva Chagas, C., Calderano Filho, B., Bhering, S.B., 2014. A regional-scale assessment of digital mapping of soil attributes in a tropical

hillslope environment. Geoderma 232–234, 479–486. https://doi.org/10.1016/j.geoderma.2014.06.007.
Castaldi, F., Palombo, A., Santini, F., Pascucci, S., Pignatti, S., Casa, R., 2016. Evaluation of the potential of the current and forthcoming multispectral and hyperspectral imagers to estimate soil texture and organic carbon. Remote Sens. Environ. 179, 54–65. https://doi.org/10.1016/j.rse.2016.03.025.
Chagas, C.da.S., de Carvalho Junior, W., Bhering, S.B., Calderano Filho, B., 2016. Spatial prediction of soil surface texture in a semiarid region using random forest and multiple linear regressions. CATENA 139, 232–240. https://doi.org/10.1016/j.catena.2016.01.001.
Clark, R.N., Swayze, G.A., Wise, R., Livo, K.E., Hoefen, T., Kokaly, R.F., Sutley, S.J., 2007. USGS digital spectral library splib06a. US Geol. Surv. Digit. data Ser. 231, 2007.
Demattê, J.A.M., Guimarães, C.C.B., Fongaro, C.T., Vidoy, E.L.F., Sayão, V.M., Dotto, A. C., Santos, N.V. dos, 2018b. Satellite Spectral Data on the Quantification of Soil Particle Size from Different Geographic Regions. Rev. Bras. Ciência do Solo.
Demattê, J.A.M., Galdos, M.V., Guimarães, R.V., Genú, A.M., Nanni, M.R., Zullo, J., 2007a. Quantification of tropical soil attributes from ETM+/LANDSAT-7 data. Int. J. Remote Sens. 28 (17), 3813–3829.
Demattê, J.A.M., Nanni, M.R., Formaggio, A.R., Epiphanio, J.C.N., 2007b. Spectral reflectance for the mineralogical evaluation of Brazilian low clay activity soils. Int. J. Remote Sens. 28, 4537–4559. https://doi.org/10.1080/01431160701250408.
Demattê, J.A.M., Fongaro, C.T., Rizzo, R., Safanelli, J.L., 2018. Geospatial Soil Sensing System (GEOS3): A powerful data mining procedure to retrieve soil spectral reflectance from satellite images. Remote Sens. Environ. 212, 161–175. https://doi.org/10.1016/j.rse.2018.04.047.
Demattê, J.A.M., Dotto, A.C., Paiva, A.F.S., Sato, M.V., Dalmolin, R.S.D., de Araújo, M.d. S.B., da Silva, E.B., Nanni, M.R., ten Caten, A., Noronha, N.C., Lacerda, M.P.C., de Araújo Filho, J.C., Rizzo, R., Bellinaso, H., Francelino, M.R., Schaefer, C.E.G.R., Vicente, L.E., dos Santos, U.J., de Sá Barretto Sampaio, E.V., Menezes, R.S.C., de Souza, J.J.L.L., Abrahão, W.A.P., Coelho, R.M., Grego, C.R., Lani, J.L., Fernandes, A. R., Gonçalves, D.A.M., Silva, S.H.G., de Menezes, M.D., Curi, N., Couto, E.G., dos Anjos, L.H.C., Ceddia, M.B., Pinheiro, É.F.M., Grunwald, S., Vasques, G.M., Marques Júnior, J., da Silva, A.J., Barreto, M.C.d.V., Nóbrega, G.N., da Silva, M.Z., de Souza, S.F., Valladares, G.S., Viana, J.H.M., da Silva Terra, F., Horák-Terra, I., Fiorio, P.R., da Silva, R.C., Frade Júnior, E.F., Lima, R.H.C., Alba, J.M.F., de Souza Junior, V.S., Brefin, M.D.L.M.S., Ruivo, M.D.L.P., Ferreira, T.O., Brait, M.A., Caetano, N.R., Bringhenti, I., de Sousa Mendes, W., Safanelli, J.L., Guimarães, C.C.B., Poppiel, R.R., e Souza, A.B., Quesada, C.A., do Couto, H.T.Z., 2019. The Brazilian Soil Spectral Library (BSSL): A general view, application and challenges Geoderma The Brazilian Soil Spectral Library (BSSL): A general view, application and challenges. Geoderma 354, 113793. https://doi.org/10.1016/j.geoderma.2019.05.043.
Demattê, J.A.M., Paiva, A.F.d.S., Poppiel, R.R., Rosin, N.A., Ruiz, L.F.C., Mello, F.A.d.O., Minasny, B., Grunwald, S., Ge, Y., Ben Dor, E., Gholizadeh, A., Gomez, C., Chabrillat, S., Francos, N., Ayoubi, S., Fiantis, D., Biney, J.K.M., Wang, C., Belal, A., Naimi, S., Hafshejani, N.A., Bellinaso, H., Moura-Bueno, J.M., Silvero, N.E.Q., 2022. The Brazilian S oil S pectral S ervice (BraSpecS): A User-Friendly System for Global Soil Spectra Communication. Remote Sens. 14 (3), 740.
Di Raimo, L.A.D.L., Amorim, R.S.S., Torres, G.N., Bocuti, E.D., Couto, E.G., 2019. Variabilidade espacial da erodibilidade no estado de Mato Grosso. Brasil. Rev. Ciências Agrárias 42, 61–70.
Di Raimo, L.A.D.L., Couto, E.G., de Mello, D.C., Demattê, J.A.M., Amorim, R.S.S., Torres, G.N., Bocuti, E.D., Veloso, G.V., Poppiel, R.R., Francelino, M.R., Fernandes-Filho, E.I., 2022. Characterizing and Modeling Tropical Sandy Soils through VisNIR-SWIR, MIR Spectroscopy, and X-ray Fluorescence. Remote Sens 14 (19), 4823. https://doi.org/10.3390/rs14194823.
Donagemma, G.K., Freitas, P.L.d., Balieiro, F.d.C., Fontana, A., Spera, S.T., Lumbreras, J. F., Viana, J.H.M., Araújo Filho, J.C.d., Santos, F.C.D., Albuquerque, M.R.d., Macedo, M.C.M., Teixeira, P.C., Amaral, A.J., Bortolon, E., Bortolon, L., 2016. Characterization, agricultural potential, and perspectives for the management of light soils in Brazil. Pesq. agropec. bras. 51 (9), 1003–1020.
Dotto, A.C., Dalmolin, R.S.D., ten Caten, A., Gris, D.J., Ruiz, L.F.C., Dotto, A.C., Dalmolin, R.S.D., ten Caten, A., Gris, D.J., Ruiz, L.F.C., 2019. AlradSpectra: a Quantification Tool for Soil Properties Using Spectroscopic Data in R. Rev. Bras. Ciência do Solo 43. https://doi.org/10.1590/18069657rbcs20180263.
Driessen, P., Deckers, J., Spaargaren, O., Nachtergaele, F., 2001. Lecture notes ont the major soils of the world, World Soil, ed. Food and Agriculture Organization (FAO), Rome.
Santos, H.G., Jacomine, P.K.T., Dos Anjos, L.H.C., De Oliveira, V.A., Lumbreras, J.F., Coelho, M.R., de Almeida, J.A., de Araujo Filho, J.C., de Oliveira, J.B., Cunha, T.J.F., 2018. Sistema brasileiro de classificação de solos. Brasília, DF: Embrapa, 2018.
EMBRAPA, 2017. Manual de metodos de analises, Manual de métodos de análise de solo.
FAO, I., 2006. ISRIC: World Reference Base for soil resource in World Soil Resource Report no. 103. FAO, Rome, Italy.
Fernandes-Filho, E.I., de Lourdes Mendonça-Santos, M., Schaefer, C.E.G.R., Dalmolin, R. S.D., Francelino, M.R., Chagas, C.S., de Carvalho Júnior, W., Demattê, J.A.M., Gomes, L.C., 2023. The Future of Brazilian Pedology: Pedometrics and Advanced Methods for Soil Survey. In: The Soils of Brazil. Springer, pp. 423–433.
Fidalski, J., Tormena, C.A., Alves, S.J., Auler, P.A.M., 2013. Influência das frações de areia na retenção e disponibilidade de água em solos das formações Caiuá e Paranavaí. Rev. Bras. Ciência do Solo 37 (3), 613–621.
Fongaro, C., Demattê, J., Rizzo, R., Lucas Safanelli, J., Mendes, W., Dotto, A., Vicente, L., Franceschini, M., Ustin, S., 2018. Improvement of clay and sand quantification based on a novel approach with a focus on multispectral satellite images. Remote Sens. 10 (10), 1555. https://doi.org/10.3390/rs10101555.
Gallo, B., Demattê, J., Rizzo, R., Safanelli, J., Mendes, W., Lepsch, I., Sato, M., Romero, D., Lacerda, M., 2018. Multi-temporal satellite images on topsoil attribute quantification and the relationship with soil classes and geology. Remote Sens. 10 (10), 1571. https://doi.org/10.3390/rs10101571.
Gasmi, A., Gomez, C., Lagacherie, P., Zouari, H., 2019. Surface soil clay content mapping at large scales using multispectral (VNIR–SWIR) ASTER data. Int. J. Remote Sens. 40, 1506–1533. https://doi.org/10.1080/01431161.2018.1528018.
Genot, V., Bock, L., Dardenne, P., Colinet, G., 2014. Use of near-infrared reflectance spectroscopy in soil analysis. A review. Biotechnol. Agron. Société Environ. 18, 247–261.
Gholizadeh, A., Žižala, D., Saberioon, M., Borůvka, L., 2018. Soil organic carbon and texture retrieving and mapping using proximal, airborne and Sentinel-2 spectral imaging. Remote Sens. Environ. 218, 89–103. https://doi.org/10.1016/j.rse.2018.09.015.
Ghrefat, H.A., Goodell, P.C., Hubbard, B.E., Langford, R.P., Aldouri, R.E., 2007. Modeling grain size variations of aeolian gypsum deposits at White Sands, New Mexico, using AVIRIS imagery. Geomorphology 88 (1-2), 57–68.
Gomez, C., Lagacherie, P., Bacha, S., 2012. Using Vis-NIR hyperspectral data to map topsoil properties over bare soils in the Cap Bon region, Tunisia. Digit. Soil Assessments Beyond 387–392. https://doi.org/10.1201/b12728-76.
Gomez, C., Adeline, K., Bacha, S., Driessen, B., Gorretta, N., Lagacherie, P., Roger, J.M., Briottet, X., 2018. Sensitivity of clay content prediction to spectral configuration of VNIR/SWIR imaging data, from multispectral to hyperspectral scenarios. Remote Sens. Environ. 204, 18–30. https://doi.org/10.1016/j.rse.2017.10.047.
Huang, J., Hartemink, A.E., 2020. Soil and environmental issues in sandy soils. Earth-Science Rev. 208, 103295 https://doi.org/10.1016/j.earscirev.2020.103295.
Hunt, G.R., 1977. Spectral signatures of particulate minerals in the visible and near infrared. Geophysics 42, 501–513. https://doi.org/10.1190/1.1440721.
Jović, B., Ćirić, V., Kovačević, M., Šeremešić, S., Kordić, B., 2019. Empirical equation for preliminary assessment of soil texture. Spectrochim. Acta - Part A Mol. Biomol. Spectrosc. 206, 506–511. https://doi.org/10.1016/j.saa.2018.08.039.
Kilmer, V.J., Alexander, L.T., 1949. Methods of making mechanical analyses of soils. Soil Sci. 68 (1), 15–24.
Kopačková, V., Ben-Dor, E., Carmon, N., Notesco, G., 2017. Modelling diverse soil attributes with visible to longwave infrared spectroscopy using PLSR employed by an automatic modelling engine. Remote Sens. 9, 134.
Krull, E., Baldock, J., Skjemstad, J., 2000. Soil Texture Effects on Decomposition and Soil Carbon Storage 103–110.
Lacerda, M., Demattê, J., Sato, M., Fongaro, C., Gallo, B., Souza, A., 2016. Tropical texture determination by Proximal Sensing using a regional spectral library and its relationship with soil classification. Remote Sens. 8 (9), 701. https://doi.org/10.3390/rs8090701.
Lehnert, L.W., Meyer, H., Obermeier, W.A., Silva, B., Regeling, B., Bendix, J., 2019. Hyperspectral Data Analysis in R : The hsdar Package. J. Stat. Softw. 89 https://doi.org/10.18637/jss.v089.i12.
Liao, K., Xu, S., Wu, J., Zhu, Q., 2013. Spatial estimation of surface soil texture using remote sensing data. Soil Sci. Plant Nutr. 59, 488–500. https://doi.org/10.1080/00380768.2013.802643.
Lumbreras, J.F., Carvalho Filho, A., Morra, P.E.F., Barros, A.H.C., Aglio, M.L.D., Dart, R., Silveira, H.L.F., Quartaroli, C.F., Almeida, R.E.M., Freitas, P.L., 2015. Aptidão Agrícola das Terras do Matopiba, 1st ed. Empresa Brasileira de Pesquisas Agropecuárias, Rio de Janeiro, RJ.
Malone, B.P., McBratney, A.B., Minasny, B., Laslett, G.M., 2009. Mapping continuous depth functions of soil carbon storage and available water capacity. Geoderma 154, 138–152. https://doi.org/10.1016/j.geoderma.2009.10.007.
Mello, D.C., Demattê, J.A.M., Mello, F.A.O., Poppiel, R., Silvero E.Q., N., Safanelli, J.L., Barros e Souza, A., Di Raimo, L.A.D, Rizzo, R., Resende,, M.E.B., Schaefer, C.G.R., 2021. Applied gamma-ray spectrometry for evaluating tropical soil processes and attributes. Geoderma 381, 114736. https://doi.org/10.1016/j.geoderma.2020.114736.
Mello, D., Demattê, J.A.M., Silvero, N.E.Q., Di Raimo, L.A.D.L., Poppiel, R.R., Mello, F.A. O., Souza, A.B., Safanelli, J.L., Resende, M.E.B., Rizzo, R., 2020. Soil magnetic susceptibility and its relationship with naturally occurring processes and soil attributes in pedosphere, in a tropical environment. Geoderma 372, 114364. https://doi.org/10.1016/j.geoderma.2020.114364.
Mello, D.C.d., Safanelli, J.L., Poppiel, R.R., Veloso, G.V., Cabrero, D.R.O., Greschuk, L.T., de Oliveira Mello, F.A., Francelino, M.R., Ker, J.C., Leite, E.P., Fernandes-Filho, E.I., Schaefer, C.E.G.R., Demattê, J.A.M., 2022a. Soil apparent electrical conductivity survey in different pedoenvironments by geophysical sensor EM38: a potential tool in pedology and pedometry studies. Geocarto Int. 37 (26), 13057–13078.
Mello, D.C.d., Veloso, G.V., Lana, M.G.d., Mello, F.A.d.O., Poppiel, R.R., Cabrero, D.R.O., Di Raimo, L.A.D.L., Schaefer, C.E.G.R., Filho, E.I.F., Leite, E.P., Demattê, J.A.M., 2022b. A new methodological framework for geophysical sensor combinations associated with machine learning algorithms to understand soil attributes. Geosci. Model Dev. 15 (3), 1219–1246.
Nanni, M.R., Demattê, J.A.M., 2006. Spectral Reflectance Methodology in Comparison to Traditional Soil Analysis. Soil Sci. Soc. Am. J. 70, 393–407. https://doi.org/10.2136/sssaj2003.0285.
Nascimento, C.M., de Sousa Mendes, W., Quiñonez Silvero, N.E., Poppiel, R.R., Sayão, V. M., Dotto, A.C., Valadares dos Santos, N., Accorsi Amorim, M.T., Demattê, J.A.M., 2021. Soil degradation index developed by multitemporal remote sensing images, climate variables, terrain and soil atributes. J. Environ. Manage. 277, 111316 https://doi.org/10.1016/j.jenvman.2020.111316.
O'Rourke, S.M., Stockmann, U., Holden, N.M., McBratney, A.B., Minasny, B., 2016. An assessment of model averaging to improve predictive power of portable vis-NIR and

XRF for the determination of agronomic soil properties. Geoderma 279, 31–44. https://doi.org/10.1016/j.geoderma.2016.05.005.
Okin, G.S., Painter, T.H., 2004. Effect of grain size on remotely sensed spectral reflectance of sandy desert surfaces. Remote Sens. Environ. 89, 272–280. https://doi.org/10.1016/j.rse.2003.10.008.
Pathak, P., Sudi, R., Wani, S.P., Sahrawat, K.L., 2013. Hydrological behavior of Alfisols and Vertisols in the semi-arid zone : Implications for soil and water management. Agric. Water Manag. 118, 12–21. https://doi.org/10.1016/j.agwat.2012.11.012.
Pereira, G.E., Sequinatto, L., De Almeida, J.A., Ten Caten, A., Mota, J.M., 2019. VIS-NIR spectral reflectance for discretization of soils with high sand content. Semin. Agrar. 40, 99–112. https://doi.org/10.5433/1679-0359.2019v40n1p99.
Poppiel, R.R., Lacerda, M.P.C., Rizzo, R., Safanelli, J.L., Bonfatti, B.R., Silvero, N.E.Q., Demattê, J.A.M., 2020. Soil color and mineralogy mapping using proximal and remote sensing in Midwest Brazil. Remote Sens. 12, 1–30. https://doi.org/10.3390/rs12071197.
Romero, D.J., Ben-Dor, E., Demattê, J.A.M., Souza, A.B.e., Vicente, L.E., Tavares, T.R., Martello, M., Strabeli, T.F., da Silva Barros, P.P., Fiorio, P.R., Gallo, B.C., Sato, M.V., Eitelwein, M.T., 2018. Internal soil standard method for the Brazilian soil spectral library: Performance and proximate analysis. Geoderma 312, 95–103.
Rosero-Vlasova, O.A., Vlassova, L., Pérez-Cabello, F., Montorio, R., Nadal-Romero, E., 2018. Modeling soil organic matter and texture from satellite data in areas affected by wildfires and cropland abandonment in Aragón, Northern Spain. J. Appl. Remote Sens. 12, 1. https://doi.org/10.1117/1.JRS.12.042803.
Rosin, N.A., Demattê, J.A.M., Poppiel, R.R., Silvero, N.E.Q., Rodriguez-Albarracin, H.S., Rosas, J.T.F., Greschuk, L.T., Bellinaso, H., Minasny, B., Gomez, C., Marques Júnior, J., Fernandes, K., 2023. Mapping Brazilian soil mineralogy using proximal and remote sensing data. Geoderma 432, 116413. https://doi.org/10.1016/j.geoderma.2023.116413.
Salazar, D.F.U., Demattê, J.A.M., Vicente, L.E., Guimarães, C.C.B., Sayão, V.M., Cerri, C.E.P., Manuela, M.C., Mendes, W.D.S., 2020. Emissivity of agricultural soil attributes in southeastern Brazil via terrestrial and satellite sensors. Geoderma 361, 114038. https://doi.org/10.1016/j.geoderma.2019.114038.
Santos, A.P., Nascimento, L.A., Pinto, S., De Sousa, R.R., 2007. Uma análise geomorfológica-hidrosedimentológica da bacia hidrográfica do córrego Aquidorobó no município de Poxoréu, estado de Mato Grosso-Brasil. Espac. y Desarro. 135–152.
Sayão, V.M., Demattê, J.A.M., Bedin, L.G., Nanni, M.R., Rizzo, R., 2018. Satellite land surface temperature and reflectance related with soil attributes. Geoderma 325, 125–140. https://doi.org/10.1016/j.geoderma.2018.03.026.
SEPLAN (State Department of Planning), 2008. Socio-Economic-Ecological Diagnosis of the State of Mato Grosso. Government of the State of Mato Grosso -. State Secretariat for Planning and General Coordination doi:CD-ROM.
Silva, E.A., Weindorf, D.C., Silva, S.H.G., Ribeiro, B.T., Poggere, G.C., Carvalho, T.S., Gonçalves, M.G.M., Guilherme, L.R.G., Curi, N., 2019. Advances in Tropical Soil Characterization via Portable X-Ray Fluorescence Spectrometry. Adv. Tropical Soil Characterization via Portable X-Ray Fluorescence Spectrometry 29 (4), 468–482.
Silvero, N.E.Q., Di Raimo, L.A.D.L., Pereira, G.S., Magalhães, L.P.d., Terra, F.d.S., Dassan, M.A.A., Salazar, D.F.U., Demattê, J.A.M., 2020. Effects of water, organic matter, and iron forms in mid-IR spectra of soils: Assessments from laboratory to satellite-simulated data. Geoderma 375, 114480. https://doi.org/10.1016/j.geoderma.2020.114480.
Silvero, N.E.Q., Demattê, J.A.M., Amorim, M.T.A., dos Santos, N.V., Rizzo, R., Safanelli, J.L., Poppiel, R.R., Mendes, W. de S., Bonfatti, B.R., 2021. Soil variability and quantification based on Sentinel-2 and Landsat-8 bare soil images: A comparison. Remote Sens. Environ. 252, 112117 https://doi.org/10.1016/j.rse.2020.112117.
Silvero, N.E.Q., Demattê, J.A.M., Minasny, B., Rosin, N.A., Nascimento, J.G., Albarracín, H.S.R., Bellinaso, H., Gómez, A.M.R., 2023. Sensing technologies for characterizing and monitoring soil functions: A review. Adv. Agron. 177, 125.
Simon, T., Zhang, Y., Hartemink, A.E., Huang, J., Walter, C., Yost, J.L., 2020. Predicting the color of sandy soils from Wisconsin, USA. Geoderma 361, 114039.
Soltani, I., Fouad, Y., Michot, D., Bréger, P., Dubois, R., Cudennec, C., 2019. A near infrared index to assess effects of soil texture and organic carbon content on soil water content. Eur. J. Soil Sci. 70 (1), 151–161.
Sousa Junior, J.G., Demattê, J.A.M., Araújo, S.R., 2011. Modelos espectrais terrestres e orbitais na determinação de teores de atributos dos solos: Potencial e custos. Bragantia 70 (3), 610–621.
Staff, S.S., 2017. Soil Survey Manual - Soil Taxonomy, Soil Survey Manual.
Stevens, A., Ramirez-Lopez, L., Stevens, M.A., Rcpp, L., 2020. Package 'prospectr.' R Packag. Version.
Sullivan, D.G., Shaw, J.N., Rickman, D., 2005. IKONOS Imagery to Estimate Surface Soil Property Variability in Two Alabama Physiographies. Soil Sci. Soc. Am. J. 69 (6), 1789–1798.
Suzuki, L.E.A.S., Pedron, F. de A., Oliveira, R.B. de, Rovedder, A.P.M., 2023. Challenges in the Management of Environmentally Fragile Sandy Soils in Southern Brazil. Soil Syst. 7, 9.
Teixeira, P.C., Donagemma, G.K., Fontana, A., Teixeira, W.G., 2017. Manual de métodos de análise de solo. Rio Janeiro, Embrapa, p. 573p.
Thanh Noi, P., Kappas, M., 2017. Comparison of random forest, k-nearest neighbor, and support vector machine classifiers for land cover classification using Sentinel-2 imagery. Sensors 18, 18.
Tucker, C.J., 1979. Red and photographic infrared linear combinations for monitoring vegetation. Remote Sens. Environ. 8 (2), 127–150.
Viscarra Rossel, R.A., Walvoort, D.J.J., McBratney, A.B., Janik, L.J., Skjemstad, J.O., 2006a. Visible, near infrared, mid infrared or combined diffuse reflectance spectroscopy for simultaneous assessment of various soil properties. Geoderma 131 (1-2), 59–75.
Viscarra Rossel, R.A., McGlynn, R.N., McBratney, A.B., 2006b. Determining the composition of mineral-organic mixes using UV-vis-NIR diffuse reflectance spectroscopy. Geoderma 137, 70–82. https://doi.org/10.1016/j.geoderma.2006.07.004.
Viscarra Rossel, R.A., Adamchuk, V.I., Sudduth, K.A., McKenzie, N.J., Lobsey, C., 2011. Proximal soil sensing: Updating the pedologist's toolkit. Adv. Agron 113, 237–282.
Rossel, R.A.V., Behrens, T., Ben-dor, E., Brown, D.J., Demattê, J.A.M., Shepherd, K.D., Shi, Z., Stenberg, B., Stevens, A., Adamchuk, V., Aïchi, H., Barthès, B.G., Bartholomeus, H.M., Bayer, A.D., Bernoux, M., Böttcher, K., Brodský, L., Du, C.W., Chappell, A., Fouad, Y., Genot, V., Gomez, C., Grunwald, S., Gubler, A., Guerrero, C., Hedley, C.B., Knadel, M., Morrás, H.J.M., Nocita, M., Ramirez-lopez, L., Roudier, P., Campos, E.M.R., Sanborn, P., Sellitto, V.M., Sudduth, K.A., Rawlins, B.G., Walter, C., Winowiecki, L.A., Hong, S.Y., Ji, W., 2016. Earth-Science Reviews A global spectral library to characterize the world ' s soil 155, 198–230. https://doi.org/10.1016/j.earscirev.2016.01.012.
Viscarra Rossel, R.A., McBratney, A.B., 1998. Laboratory evaluation of a proximal sensing technique for simultaneous measurement of soil clay and water content. Geoderma 85 (1), 19–39.
Wang, S., Li, W., Li, J., Liu, X., 2014. Prediction of Soil Texture Using FT-NIR Spectroscopy and PXRF Spectrometry With Data Fusion 178, 626–638. https://doi.org/10.1097/SS.0000000000000026.
Xiao, J., Shen, Y., Tateishi, R., Bayaer, W., 2006. Development of topsoil grain size index for monitoring desertification in arid land using remote sensing. Int. J. Remote Sens. 27, 2411–2422. https://doi.org/10.1080/01431160600554363.
Yost, J.L., Hartemink, A.E., 2019. Soil organic carbon in sandy soils: A review. Adv. Agron. 158, 217–310.
Zhang, L., Han, J., 2019. Improving water retention capacity of an aeolian sandy soil with feldspathic sandstone. Sci. Rep. 1–8 https://doi.org/10.1038/s41598-019-51257-y.
Zhu, Y., Weindorf, D.C., Zhang, W., 2011. Characterizing soils using a portable X-ray fluorescence spectrometer: 1. Soil texture. Geoderma 167–168, 167–177. https://doi.org/10.1016/j.geoderma.2011.08.010.